NASA TECHNICAL NOTE

NASA TN D-6919

NASA TN D-6919

LOW SPEED AERODYNAMIC CHARACTERISTICS OF A LARGE-SCALE MODEL WITH A THIN, HIGHLY SWEPT, 2.67 ASPECT RATIO WING HAVING A CRANKED LEADING EDGE

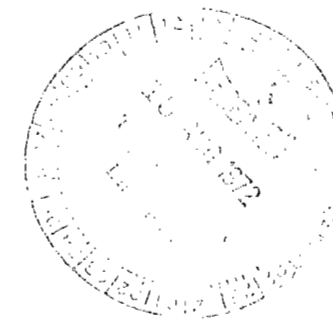

by Demo J. Giulianetti and Ralph L. Maki

Ames Research Center
Moffett Field, Calif. 94035

NATIONAL AERONAUTICS AND SPACE ADMINISTRATION • WASHINGTON, D. C. • AUGUST 1972

1. Report No. NASA TN D-6919	2. Government Accession No.	3. Recipient's Catalog No.
4. Title and Subtitle LOW SPEED AERODYNAMIC CHARACTERISTICS OF A LARGE-SCALE MODEL WITH A THIN, HIGHLY SWEPT, 2.67 ASPECT RATIO WING HAVING A CRANKED LEADING EDGE		5. Report Date August 1972 6. Performing Organization Code
7. Author(s) Demo J. Giulianetti and Ralph L. Maki		8. Performing Organization Report No. A-3893 10. Work Unit No. 760-74-07-01-00-21
9. Performing Organization Name and Address Ames Research Center Moffett Field, Calif., 94035		11. Contract or Grant No. 13. Type of Report and Period Covered Technical Note
12. Sponsoring Agency Name and Address National Aeronautics and Space Administration Washington, D. C. 20546		14. Sponsoring Agency Code

15. Supplementary Notes

16. Abstract

The low speed aerodynamic characteristics of a large-scale model intended to represent advanced fixed-wing fighters have been investigated in the Ames 40- by 80-Foot (12.2- by 24.4-m) Wind Tunnel. The model possessed positive static longitudinal stability to nearly 28° angle of attack, the maximum tested, both with and without leading-edge flaps deflected. Lateral control with differentially deflected ailerons and a right wing spoiler simultaneously deployed as combined controls was only slightly greater than that with the differentially deflected ailerons deployed as a separate control without the spoiler. Measured lift and drag were in close agreement with that predicted by theory to about 14° angle of attack, including the prediction of lift due to 30° of trailing edge flap deflection. Estimated takeoff performance of an aircraft 4/3 the scale of the test model showed takeoff distances of less than 610 m (2000 ft).

17. Key Words (Suggested by Author(s)) Low-speed aerodynamics Stability and control High-speed fighter aircraft Flaps	18. Distribution Statement Unclassified – Unlimited		
19. Security Classif. (of this report) Unclassified	20. Security Classif. (of this page) Unclassified	21. No. of Pages 44	22. Price* $3.00

* For sale by the National Technical Information Service, Springfield, Virginia 22151

NOTATION

In conformance with NASA policy, the International System of Units (SI) is used in this report. However, to make the data and other information presented herein more readily useful, dimensional quantities are indicated parenthetically in U. S. Customary Units which are commonly used in engineering practice in the aircraft industry of the United States. Measurements were made in U. S. Customary Units and equivalent SI units were determined by using conversion factors given in reference 1.

b	span of wing, m (ft)
$\bar{c}$	mean aerodynamic chord, m (ft)
C_D	drag coefficient, $\frac{D}{qS}$
C_{D_0}	drag coefficient at 0° angle of attack
C_L	lift coefficient, $\frac{L}{qS}$
C_{L_0}	lift coefficient at 0° angle of attack
C_{L_α}	lift-curve slope
ΔC_{L_f}	incremental lift coefficient due to trailing-edge flap deflection
C_l	rolling-moment coefficient, $\frac{rolling\ moment}{qSb}$
C_m	pitching-moment coefficient, $\frac{pitching\ moment}{qS\bar{c}}$
C_n	yawing-moment coefficient, $\frac{yawing\ moment}{qSb}$
C_Y	side-force coefficient, $\frac{Y}{qS}$
D	drag, N (lb)
i	horizontal-tail incidence relative to fuselage, deg
mc	moment center
q	free-stream dynamic pressure, N/m^2 (psf)
R	Reynolds number, $\frac{V\bar{c}}{\nu}$
S	wing area, m^2 (sq ft)

V	free-stream velocity, m/sec (ft/sec or knots)
y	spanwise distance normal to fuselage centerline, m (ft)
Y	side force, N (lb)
α	fuselage angle of attack, deg
β	sideslip angle, deg
γ	flight-path angle, deg
δ	flap or spoiler deflection, deg
Δ	incremental value
ϵ	downwash angle, deg
η	fraction semispan, $\frac{y}{b/2}$
ν	free-stream kinematic viscosity, m^2/sec (ft^2/sec)

Subscripts

a	aileron
f	trailing-edge flaps
GEAR	main and nose wheel gear
IGE	in ground effect
l	left
N	leading-edge flaps
OGE	out of ground effect
r	right or rotation
s	spoiler

Examples of Flap, Aileron, and Spoiler Deflection

$\delta_N = 50°/35°$	inboard leading-edge flap span at 50° and outboard leading-edge flap span at 35°
$\delta_f = 30°$	inboard trailing-edge flap span at 30° and outboard trailing-edge flap span at 0°
$\frac{\delta_{a_l}}{\delta_{a_r}} = 20°/-20°$	outboard trailing-edge flaps deflected ±20° (total of 40°) as ailerons. Positive total deflection and positive roll (right wing down) when the outboard flap trailing edges are down on the left flap and up on the right flap
$\delta_s = 40°$	spoiler deflected 40° on the outboard right wing panel (spoiler removed from wing when undeflected ($\delta_s = 0°$))

LOW SPEED AERODYNAMIC CHARACTERISTICS OF A LARGE–SCALE MODEL WITH A THIN, HIGHLY SWEPT, 2.67 ASPECT RATIO WING HAVING A CRANKED LEADING EDGE

Demo J. Giulianetti and Ralph L. Maki

Ames Research Center

SUMMARY

The low speed aerodynamic characteristics of a large-scale model intended to represent advanced fixed-wing fighters have been investigated in the Ames 40– by 80–Foot (12.2– by 24.4–m) Wind Tunnel. The model possessed positive static longitudinal stability to nearly 28° angle of attack, the maximum tested, both with and without leading-edge flaps deflected. Lateral control with differentially deflected ailerons and a right wing spoiler simultaneously deployed as combined controls was only slightly greater than that with the differentially deflected ailerons deployed as a separate control without the spoiler. Measured lift and drag were in close agreement with that predicted by theory to about 14° angle of attack, including the prediction of lift due to 30° of trailing edge flap deflection. Estimated takeoff performance of an aircraft 4/3 the scale of the test model showed takeoff distances of less than 610 m (2000 ft).

INTRODUCTION

The performance requirements of certain current fighter aircraft designs dictate a high degree of maneuverability at transonic and supersonic cruise speeds. These designs often incorporate thin, highly swept, low aspect ratio wings and propulsive systems with high thrust-to-weight ratios having inlets located at or near the fuselage-wing leading edge juncture. Such configurations are characterized by strong lift and stability changes due to wing leading edge vortex flow as well as wing flow field changes due to vortices shed from the inlet leading edges. Further, potential flow theory does not account for the flow phenomena associated with the strong leading edge vortices.

The present 40– by 80–foot (12.2–by 24.4–m) wind tunnel investigation was made to explore the low-speed aerodynamic problems associated with this type of design and to document the longitudinal and lateral-directional aerodynamic characteristics. The large-scale model was configured to represent a typical high-speed aircraft developed in a general study by the NASA on advanced high-speed fighter concepts. General longitudinal and lateral-directional aerodynamic characteristics were determined for a range of leading- and trailing-edge flap deflections as was the longitudinal control power of variable incidence horizontal tails and the lateral control power of ailerons alone and in combination with a right wing spoiler. A comparison of measured results with those predicted by theory was made. The takeoff performance of the full scale aircraft (4/3 the scale of the test model was estimated and included the power effects of an engine failure during takeoff.

Six component force and moment data were obtained for a range of angles of attack to nearly 28° and for sideslip angles to 7° at Reynolds numbers ranging from 9.7 to 19.3 million based on a wing mean aerodynamic chord of 4.34 m (14.25 ft).

MODEL DESCRIPTION

General

Photographs of the model installed in the test section of the Ames 40– by 80–Foot (12.2– by 24.4–m) Wind Tunnel are shown in figure 1. Model geometry and additional model dimensional data are given in figure 2 and table 1. Figure 3 is a sketch of the total lifting planform used in the theoretical comparisons; figure 4 and table 2 give pertinent information on the full scale aircraft assumed for the takeoff performance estimates.

Wing

Wing planform geometry is shown in figure 2(a). The wing had an aspect ratio of 2.67; a taper ratio of 0.18; and a symmetrical, 4 percent thick, biconvex section with no camber or twist. The leading edge was cranked at $\eta = 0.645$ and had sweep angles of 56.5° and 37°, respectively, for the inboard and outboard wing panels. The wing was mounted at 1.8° of incidence with respect to the fuselage.

Wing High Lift Devices

Leading- and trailing-edge flaps were deflected in two spanwise sections. The inboard flap span extended from $\eta = 0.24$ to $\eta = 0.645$ and the outboad flap span extended from $\eta = 0.645$ to $\eta = 0.96$ for both the leading- and trailing-edge flaps.

Leading-edge flaps– The leading-edge flaps are shown in figure 2(b). Streamwise flap to wing chord ratios for the inboard flap ranged from 0.20 at $\eta = 0.24$ to 0.29 at $\eta = 0.645$ and were a constant 0.29 for the outboard flap. Flap deflections ranged from 0° over the entire span, the cruise configuration, to $\delta_N = 50°/35°$, the high lift configuration. The majority of testing was done with the flaps in the high lift configuration.

Trailing-edge flaps– The trailing-edge flaps are shown in figure 2(c). Streamwise flap to wing chord ratios for the trailing-edge flaps varied from 0.15 at $\eta = 0.24$ to 0.18 at $\eta = 0.645$. The flaps were single slotted with a slot to wing chord ratio varying from 0.001 at $\delta_f = 10°$ to 0.005 at $\delta_f = 40°$ measured normal to the hinge line.

Ailerons

The outboard trailing-edge flaps were deployed as ailerons for roll control by differential deflection of the left- and right-hand segments (fig. 2(d)). They were unslotted and had a streamwise aileron to wing chord ratio of 0.18 that was constant for the aileron span extending from $\eta = 0.645$ to $\eta = 0.96$.

Spoiler

The spoiler used in this investigation is shown in figure 2(d) and was located on the outboard right wing panel only. It had a span extent from $\eta = 0.645$ to $\eta = 0.96$ and a constant spoiler to streamwise wing chord ratio of 0.10. The spoiler was positioned on the wing so that the spoiler trailing edge terminated at the 0.82 percent wing chord station at 0° spoiler deflection and was removed from the wing for the undeflected spoiler ($\delta_S = 0°$) investigations.

Tails

The geometry of the twin vertical and horizontal tails is shown in figure 2(a). The horizontal and vertical tails had symmetrical, 4 percent thick, biconvex sections. The vertical tails were fixed in an 8° outboard canted position while the horizontal tails were movable within a variable incidence range of −20° to +25° (negative incidence was leading edge down).

Inlets

The two-dimensional inlets are shown in figure 2(a). They had sharp leading edges extending ahead of the wing leading edge, and were located at the fuselage-wing juncture and faired directly into the wing contour. The model was ducted for through cold flow, which exited at the rear of the fuselage.

TESTS AND PROCEDURE

The general method of testing was to vary angle of attack or sideslip at constant forward speed for selected configurations. Force and moment data were obtained for a range of Reynolds numbers from 9.7×10^6 to 19.3×10^6 based on a wing mean aerodynamic chord of 4.34 m (14.25 ft) and free-stream dynamic pressures ranging from 656 to 2,575 N/sq m (13.7 to 53.8 lb/sq ft). Most six-component data were obtained at a Reynolds number of 16.4×10^6 corresponding to a dynamic pressure of 1852 N/sq m (38.7 lb/sq ft). Angle of attack was varied from approximately −8° to 28° at 0° sideslip, and sideslip was varied from 0° to 7° at 0.2° and 12.9° angle of attack.

CORRECTIONS

Standard corrections for wind-tunnel wall effects and strut tare corrections to account for wind effects on the exposed portions of the model support struts were applied to the data as follows:

$$\alpha = \alpha_{uncorrected} + \Delta\alpha_{tunnel\ wall}$$

$$C_D = C_{D_{uncorrected}} + \Delta C_{D_{tunnel\ wall}} - \Delta C_{D_{strut\ tare}}$$

$$C_m = C_{m_{uncorrected}} + \Delta C_{m_{tunnel\ wall}} - \Delta C_{m_{strut\ tare}}$$

yielding the corrections:

	Wind tunnel wall	Strut tare
$\Delta\alpha$	$0.969\ C_L$	---
ΔC_D	$0.0155\ C_L^2$	0.0022
ΔC_m	$0.0077\ C_L$	−.0006

RESULTS AND DISCUSSION

The results of the investigation are presented in figures 5 through 17. These figures are indexed in table 3.

Longitudinal Aerodynamic Characteristics

The longitudinal aerodynamic characteristics of the model are presented in figures 5(a) and (b) for a range of forward speeds from 33 m/sec to 65 m/sec (63 knots to 126 knots). These results are for the cruise and high-lift configurations and show no significant changes with variation in Reynolds number and velocity.

Effects of leading-edge flap deflection– The effects of varying deflection on the inboard and outboard leading-edge flap segments are shown in figure 6(a). Deflecting the leading-edge flaps resulted in a loss in lift throughout the angle-of-attack range to about 21°. Tuft observations indicated that the nonlinearity of the lift curves at the higher angles of attack for some of the intermediate leading-edge flap deflections was probably due to unsteady flow that spread spanwise with increased angle of attack. This unsteady flow was related to separation behind the vortices

shed from the inlet leading edges and the wing cranked leading-edge junctures. The most effective leading-edge configuration tested, and the one chosen for this investigation, was 50° inboard and 35° outboard ($\delta_N = 50°/35°$) with the leading-edge slot sealed. Although lift over most of the angle-of-attack range was below that of the flaps-up configuration, the lift-curve slope was nearly linear to 28° angle of attack, with the lift being higher above 21° angle of attack. This configuration maintained positive static stability and a linear pitching-moment variation throughout the angle-of-attack range tested. Leading-edge flap deflection generally reduced the level of drag at the angles of attack of interest for takeoff and landing.

Figure 6(b) shows the effects of sealing the leading-edge flap slot on a 50°/35° high-lift configuration in an attempt to reduce the pressure gradients over the knee of the flap. These effects were investigated only with a bulbous leading edge (fig. 2(b)); however, the incremental effects were assumed to apply with a sharp leading edge. Although the bulbous leading edge resulted in some increase in lift coefficient beyond about 16° angle of attack, accompanied by a slight reduction in drag, this configuration was not investigated further since it was not considered practical for high-speed flight. Sealing the leading-edge slot resulted in increased lift and some reduction of drag over the entire angle-of-attack range and a slight decrease in stability. Unless otherwise noted, the remainder of the investigation was made with a sharp leading edge and the flap slot sealed when the leading edge flaps were deflected.

Effects of horizontal-tail incidence– The effects of varying the horizontal tail incidence on the model longitudinal aerodynamic characteristics are shown in figures 7(a) and (b) for the cruise and high-lift configurations. The effectiveness of the horizontal tails as a longitudinal trim and control device in terms of ΔC_m for the cruise configuration was linear and was maintained throughout the incidence range tested of −20° to 25° at both 0.2° and 12.8° angle of attack (fig. 7(a)).

Trailing-Edge Flap Effectiveness

The effects of deflecting the trailing-edge flaps through a range of flap angles to 40° on the model longitudinal aerodynamic characteristics are shown in figures 8(a) and (b) for the model with the horizontal tails on and removed. Trailing-edge flap effectiveness in terms of ΔC_L due to flap deflection is shown in figure 9 for 0.28° angle of attack and compared with the flap lift predicted by the theory of reference 2. Flap lift was a maximum with 30° of trailing-edge flap deflection (figs. 8(a), 8(b), and 9); it was in good agreement with the theory of reference 2 to about 25° of flap deflection but was less than that predicted by the theory at flap deflections greater than about 25° (fig. 9). Tuft observations with the trailing-edge flaps deflected showed areas of rough, spanwise flow at low angles of attack at the inboard and outboard extremities of the flap spans in line with the vortices shed from the inlet leading edges and the cranked wing leading-edge junctures. These vortices induced rough, spanwise flow, which spread inward over the flaps as angle of attack was increased. However, flap effectiveness was only slightly affected since the force data showed that the flap lift increment was maintained to high angles of attack.

Effects of horizontal tails– Downloads on the horizontal tails induced by downwash from the deflected trailing-edge flaps significantly reduced flap lift (fig. 9). Figure 10 shows the incremental contribution of the horizontal tails to lift, drag, and pitching moment for 0° and 30° of trailing-edge flap deflection. Estimates of the effective downwash from 30° of trailing-edge flap

deflection, based on the data of figure 7, are given in figure 11. The results show downwash angles at the horizontal tails for the high-lift configuration ranging from about 10.5° at $\alpha = 0°$ to about 15.4° at $\alpha = 15°$.

Comparisons With Theory

Theoretical estimates of the model lift and drag based on the theories of references 2 and 3 are compared with the measured model lift and drag characteristics in figures 12(a) and (b). The theory of reference 2 is an improved version of lifting surface theory that assumes full leading-edge suction and which accounts for changes in span loading due to discontinuities on the wing leading edge and estimates the lift increment due to trailing-edge flap deflection. This theory was also used to estimate the lift and drag of the model when the aft fuselage area, shown as the shaded area in figure 3, was included as part of the total lifting surface. The theory of reference 3 estimates the total wing lift as the sum of potential flow lift with no leading-edge suction and vortex lift with full leading-edge suction. A delta wing with a thin, sharp leading edge having the same aspect ratio as the model wing was assumed for the application of the theory of reference 3. Differences between measured results and those estimated from theory can be attributed, in part, to flow separation effects, such as at the wing tips and behind the vortices shed from the inlet and cranked wing leading edges, not accounted for by theory which assumes potential flow over the wing.

Lift– The theoretical lift predictions, although slightly lower than the measured lift, were in good agreement with the measured lift-curve slope to about 14° angle of attack for the trailing-edge flaps undeflected (figs. 12(a) and (b)) and deflected 30° (fig. 12(a)), and would indicate nearly potential flow conditions at the wing leading edges to these angles of attack. The best agreement of measured lift with that predicted by the theory of reference 2 occurred when the aft fuselage section was included as part of the total lifting planform (fig. 12(a)). The flap lift increment predicted by this theory at 0° angle of attack is about 15 percent larger than the measured value (fig. 12(a)). The approximate 1° shift in angle of attack for zero lift for the measured data with trailing-edge flaps undeflected, shown in figure 12(a), has not been explained.

Drag– The theoretical estimates of induced drag (refs. 2 and 3) were added to the measured model C_{D_0} of 0.02 and 0.06, respectively, for the trailing-edge flaps undeflected and deflected 30° (fig. 8(b)), and are compared with the measured drag in figures 12(a) and (b). The drag predicted from the theories of references 2 and 3 with full leading-edge suction closely estimated the measured drag to about 14° angle of attack (figs. 12(a) and (b)), beyond which flow separation resulted in losses in lift and accompanying increases in drag. This also indicated that the wing leading edges were operating with essentially potential flow conditions to about this angle of attack. As would be expected, there was little change in the estimated drag when the aft fuselage section was included in the total lifting surface (fig. 12(a)).

Lateral-Directional Aerodynamic Characteristics

Directional stability– The vertical-tail volume was sufficient for directional stability to 7° sideslip, the maximum investigated, for both the cruise and high-lift configurations at 0.2° and 12.9° angle of attack (figs. 13(a) and (b)). Tuft observations showed that the loss in directional

stability (C_{n_β}) at 12.9° angle of attack (fig. 13(b)) may have been due, in part, to the effects of sidewash flow on the outboard surfaces of the vertical tails induced by the vortices shed from the inlet leading edges and the wing leading edge-inlet junctures at the higher angles of attack.

Lateral-directional control– Differentially deflected ailerons and a spoiler on the outboard right wing panel (fig. 2(d)) were investigated as lateral control devices, both as isolated and combined controls, for a range of angles of attack to about 28° and of sideslip to 7° (the maximum investigated). These results are presented in figures 14(a) and (b), and 15 for the model with the ailerons differentially deflected ±20° on the left and right wing panels, respectively (total of 40° deflection, see notation section), and with a spoiler deflection of 40°. The results of figure 15 were used to determine the effectiveness of ±20° of differential aileron deflection and 40° of right wing spoiler deflection in terms of incremental changes in rolling-moment coefficient with changes in angle of attack. These results are presented in figure 16 for the ailerons and spoiler deployed both as separate and combined controls at 0° sideslip and show that control effectiveness decreased with increases in angle of attack beyond about 8°. The effectiveness of the ailerons and the spoiler, when deployed as separate controls at 0° sideslip, decreased to zero near 25° angle of attack (fig. 16). As might be expected, the effects of simultaneous deployment of ailerons and spoiler are quite different than would be estimated by the simple addition of the effects measured as individual controls.

Estimated Takeoff Performance

High performance fighter aircraft designs utilizing thin, highly swept, fixed wings will be typically characterized by high installed thrust and moderate design wing loadings (from about 296 kg/sq m (60 lb/sq ft) to about 395 kg/sq m (80 lb/sq ft)) and, as a result, the low speed maximum lift requirements should not be severe. The measured longitudinal aerodynamic characteristics for the present model in the high lift configurations shown in figure 6(a) suggest nothing unusual about the approach and landing speeds. However, the approach speed would have to be about 1.25 times the stall speed to provide a reasonable attitude for tail clearance. At this approach speed, the aircraft would be landing on the backside of the thrust required curve. A more effective trailing-edge flap may be desirable to permit lower approach speeds without tail bumping.

An investigation was made of the takeoff performance at high T/W of an aircraft of the same configuration as the test model. The full scale aircraft was 4/3 the scale of the test model and had a wing loading at takeoff of 296 kg/sq m (60 lb/sq ft), considered to represent the low end of a probable range of takeoff gross weights. Table 2 lists the parameters assumed for the aircraft in estimating the takeoff performance. The aircraft was assumed to have 6.1 percent positive static longitudinal stability ($dC_m/dC_L = -0.061$) based on neutral static longitudinal stability at 0.319 $\bar{c}$ (figs. 4 and 7(b)).

Computer program– A digital computer program (described in an unpublished Ames report by V. Corsiglia) was used to estimate the takeoff performance, which comprised ground roll, rotation, transition from rotation to lift-off, lift-off, and climbout phases. A maximum rotation angle of 14° was used to avoid tail bump at rotation (fig. 4), and a constant pitch attitude of 23° was selected as the mode of climbout. The program was capable of estimating the effects of engine failure and ground proximity during the ground roll and from rotation to climbout. The measured data of figure 7(b) used for the takeoff analysis were adjusted for ground effect as shown in table 2

and were presumed to apply to the aircraft. The ground effects were estimated from measured, unpublished data of a large-scale model with a 1.7 aspect ratio wing having a cranked leading edge with inboard and outboard leading-edge sweep angles of 74.2° and 54°, respectively. The aircraft was assumed to be out of ground effect at a 6.1 m (20-foot) height, at which time the computer program accounted for the effects of partial gear retraction from fully extended to fully retracted and adjusted C_D accordingly.

Method used to estimate takeoff– The method used to estimate takeoff performance was to minimize the forward speed required for rotation consistent with a maximum horizontal-tail deflection of −30°. The computational technique involved the application of full horizontal-tail deflection for a range of forward speeds at rotation until a minimum rotation speed was established. The program then iterated with lesser values of horizontal-tail deflection until trim in climbout was achieved without exceeding an assumed limit aircraft rotation rate ($d\alpha/dt$) of 0.5°/sec and an assumed limit horizontal-tail deflection rate of 10°/sec.

Takeoff performance– The estimated takeoff performance characteristics of the full scale aircraft are shown in figures 17(a) and (b) for a maximum performance takeoff (with afterburners, $T/W = 1$), including the effects of an engine failure at rotation, and for a normal takeoff (without afterburners, $T/W = 0.5$). It was assumed that rudder power would be adequate to overcome any directional instability arising from the thrust asymmetry due to the failure of one engine without altering the drag characteristics of the airplane. These results show that the times required from the start of takeoff to a 15.2-m (50-ft) height varied from 10.6 sec for a maximum performance takeoff to 16.8 sec for a normal takeoff (fig. 17(a)). The high takeoff performance of the aircraft is further illustrated by the short distances that accompanied the short times required to reach a 15.2-m (50-ft) height. These distances ranged from 532 m (1744 ft) for a maximum performance takeoff to 750 m (2461 ft) for a normal takeoff (fig. 17(a)) with corresponding flight path angles at a 15.2-m (50-ft) height of 11° and 8.4°, respectively (fig. 17(b)). The failure of one engine at minimum rotation velocity during a maximum performance takeoff resulted in little loss in takeoff performance. The resulting thrust loss was assumed complete in 2.5 sec (program input) fig. 17(b)), and the remainder of the takeoff to a 15.2-m (50-ft) height was accomplished with the remaining engine with the afterburner in 2.5 sec from the time of complete thrust loss (fig. 17(a)). The takeoff time and distance to a 15.2-m (50-ft) height for the engine-out case were 11.4 sec and 571 m (1873 ft), respectively, with a flight path angle of 8.6° at the15.2-m (50-ft) height (figs. 17(a) and (b)).

CONCLUSIONS

Theoretical estimates of lift and drag using lifting surface and vortex lift prediction methods were in close agreement with measured lift and drag to about 14° angle of attack with the trailing-edge flaps undeflected and indicated near potential flow conditions at the wing leading edges to these angles of attack. The lifting surface prediction method, best when the total lifting surface was considered, also closely predicted the lift and drag with 30° of trailing-edge flap deflection.

Estimates of the takeoff performance of an aircraft with the same configuration as the test model and assumed to be 4/3 the scale of the test model showed very short times and distances

required to reach a 15.2-m (50-ft) height. The failure of one of two engines at rotation resulted in little loss in takeoff performance. Takeoff distances were less than 762 m (2500 ft).

Lift coefficient increased to nearly 28° angle of attack, the maximum tested, for the high lift configuration and to nearly 26° angle of attack for the cruise configuration without reaching a maximum value and was accompanied by positive static longitudinal stability throughout these angle-of-attack ranges for both the cruise and high lift configurations.

Some loss in directional stability at high angles of attack appeared to result from sidewash on the vertical tails from vortices shed from the inlet leading edges.

Ames Research Center
National Aeronautics and Space Administration
Moffett Field, Calif., 94035, March 24, 1972

REFERENCES

1. Mechtly, E. A.: The International System of Units. NASA SP–7012, 1964.

2. Wagner, Siegfried: On the Singularity Method of Subsonic Lifting-Surface Theory. J. Aircraft, vol. 6, no. 6, Nov. – Dec. 1969, pp. 549–558.

3. Polhamus, Edward C.: A Concept of the Vortex Lift Of Sharp-Edge Delta Wings Based on a Leading-Edge Suction Analogy. NASA TN D–3767, 1966.

TABLE 1.– MODEL DIMENSIONAL DATA

Wing	
Area, m^2 (sq ft)	37.9 (407.8)
Span, m (ft)	10.1 (33)
Tip chord, m (ft)	1.3 (4.3)
Root chord at fuselage $\mathcal{L}$, m (ft)	7.3 (23.9)
Mean aerodynamic chord, m (ft)	4.3 (14.25)
Leading edge sweep angle, deg	
Inboard panel	56.5
Outboard panel	37
Aspect ratio	2.67
Taper ratio	0.18
Incidence relative to fuselage, deg	1.8
Airfoil section, streamwise	Symmetrical, biconvex
Thickness ratio, streamwise, percent chord	4
Horizontal tails	
Number of panels	2
Exposed area for one panel, m^2 (sq ft)	3.5 (37.8)
Tip chord, m (ft)	1.2 (4)
Root chord at tail boom $\mathcal{L}$, m (ft)	2.7 (9)
Leading-edge sweep angle, deg	49
Airfoil section, streamwise	Symmetrical, biconvex
Thickness ratio, percent chord	4
Vertical tails	
Number of panels	2
Exposed area for one panel, m^2 (sq ft)	1.7 (29.1)
Tip chord, m (ft)	0.7 (2.25)
Root chord at tail boom reference line projected 8° (see fig. 2(a)), m (ft)	3.3 (10.72)
Leading-edge sweep angle, deg	56.5
Airfoil section, streamwise	Symmetrical, biconvex
Thickness ratio, percent chord	4
Outward cant relative to the vertical, deg	8

TABLE 2.– PARAMETER INFORMATION FOR THE FULL SCALE AIRCRAFT

Wing	
Area, m^2 (sq ft)	67.3 (725)
Span, m (ft)	13.4 (44)
Mean aerodynamic chord, m (ft)	5.8 (19)
Aircraft	
Gross weight, kg (lb)	19,732 (43,500)
Number of engines	2
Thrust-to-weight ratio (T/W)	
With afterburners	1
Without afterburners	0.5
Moment of inertia in pitch about aircraft cg, kg-m^2 (slug-ft^2)	257,604 (190,000)
Miscellaneous	
Coefficient of rolling friction	0.02
Drag coefficient of gear fully extended	0.012
Height out-of-ground effect, m (ft)	6.1 (20)
Specific fuel consumption, kg fuel/hr/N (lb fuel/hr/lb thrust)	
With afterburners	1 (2.2)
Without afterburners	0.4 (1)
$C_{L_{IGE}} = 1.059\, C_{L_{OGE}}$	
$C_{D_{IGE}} = 0.832\, C_{D_{OGE}} + C_{D_{GEAR}}$	
$C_{M_{IGE}} = 1.214\, C_{M_{OGE}}$	

TABLE 3.– INDEX TO FIGURES

Figure	Description	δ_N, deg	δ_f, deg	α, deg	β, deg
1	Model photographs				
2	Model geometry				
3	Wing planform showing total lifting area for theoretical comparisons				
4	Sketch showing center-of-gravity locations and ground roll attitude of the full scale aircraft used to estimate takeoff performance				
	Longitudinal aerodynamic characteristics				
5	Effect of Reynolds number variation	0,50/35	0,30	var	0
6	Effect of leading-edge flap deflection	var	30	var	0
7	Effect of horizontal-tail incidence changes and of the horizontal tails on longitudinal stability	0, 50/35	0,30	var, 0.2 12.8	0
8	Effect of trailing-edge flap deflection with horizontal tails installed and removed	0	var	var	0
9	Effect of horizontal tails on trailing-edge flap effectiveness	0	var	0.28	0
10	Effect of trailing-edge flap deflection on the incremental contribution of the horizontal tails	0	0, 30	var	0
11	Estimated downwash at the horizontal tails	50/35	30	var	0
12	Comparison of measured and theoretical estimates of lift and drag characteristics	0	0, 30	var	0
	Lateral-directional aerodynamic characteristics				
13	Vertical-tail contribution to directional stability	0, 50/35	0,30	0.2 12.9	var
14	Effect of aileron and right wing spoiler deflection with changes in sideslip	50/35	30	0.2, 12.9	var
15	Effect of aileron and right wing spoiler deflection with changes in angle of attack	50/35	30	var	0, –7
16	Effect of aileron and right wing spoiler deflection on incremental changes in rolling moment	50/35	30	var	0, –7
	Performance				
17	Estimated takeoff performance characteristics.				

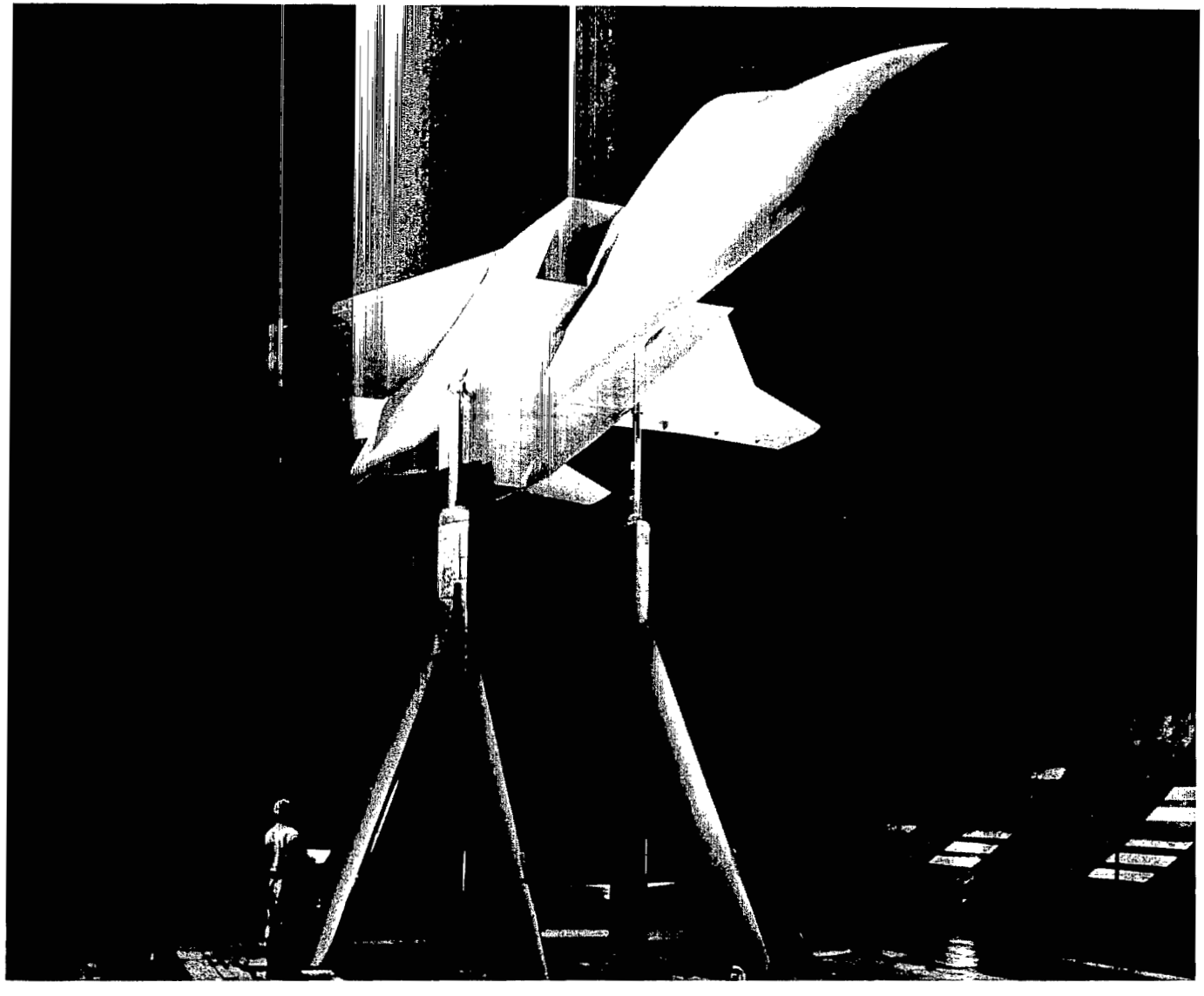

(a) Cruise configuration; $\delta_N = 0°$, $\delta_f = 0°$.

Figure 1.– Model mounted in the test section of the Ames 40– by 80–Foot (12.2– by 24.4–m) Wind Tunnel; $i = 0°$.

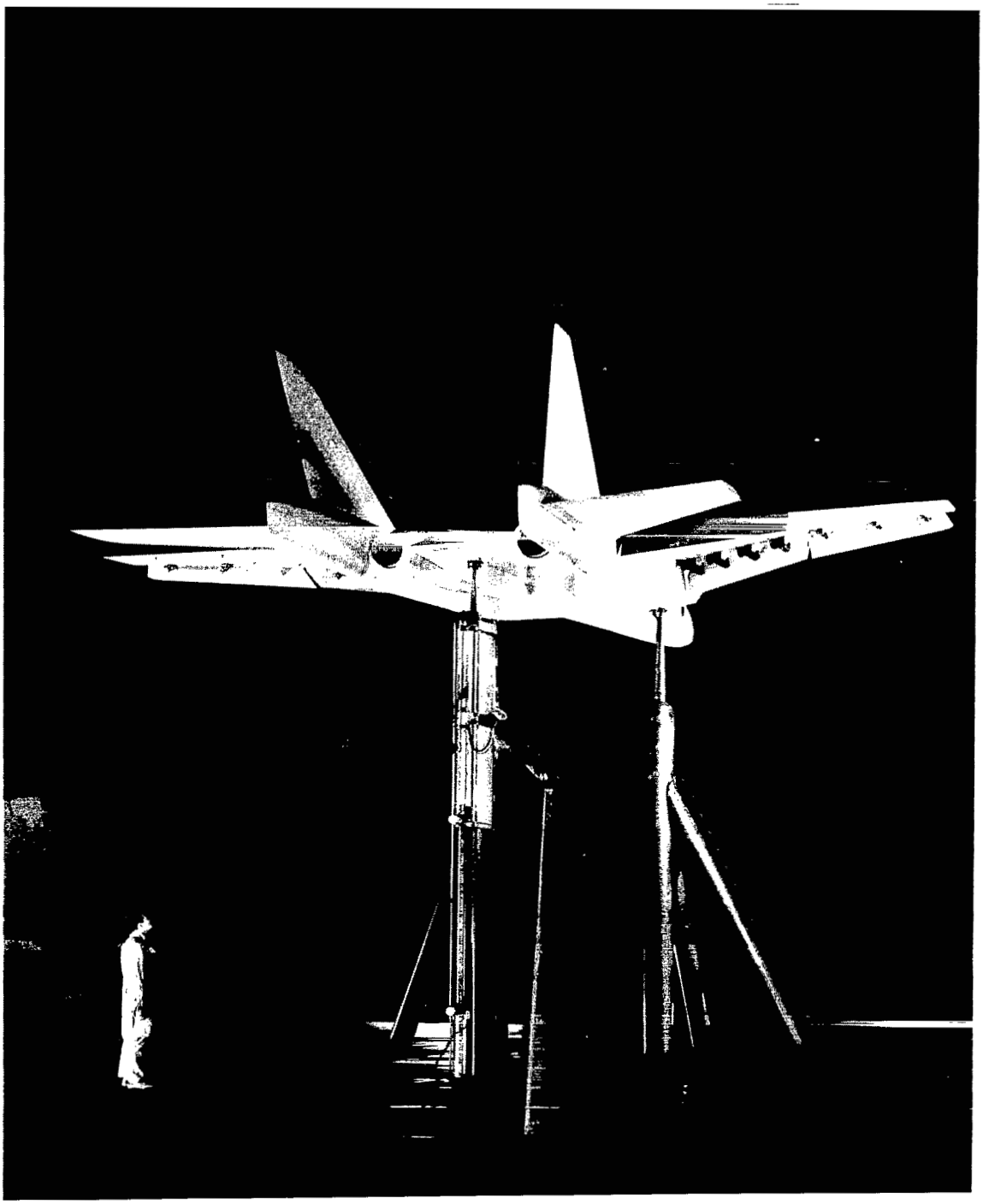

(b) High-lift configuration; $\delta_N = 50°/35°$, $\delta_f = 30°$.

Figure 1.– Concluded.

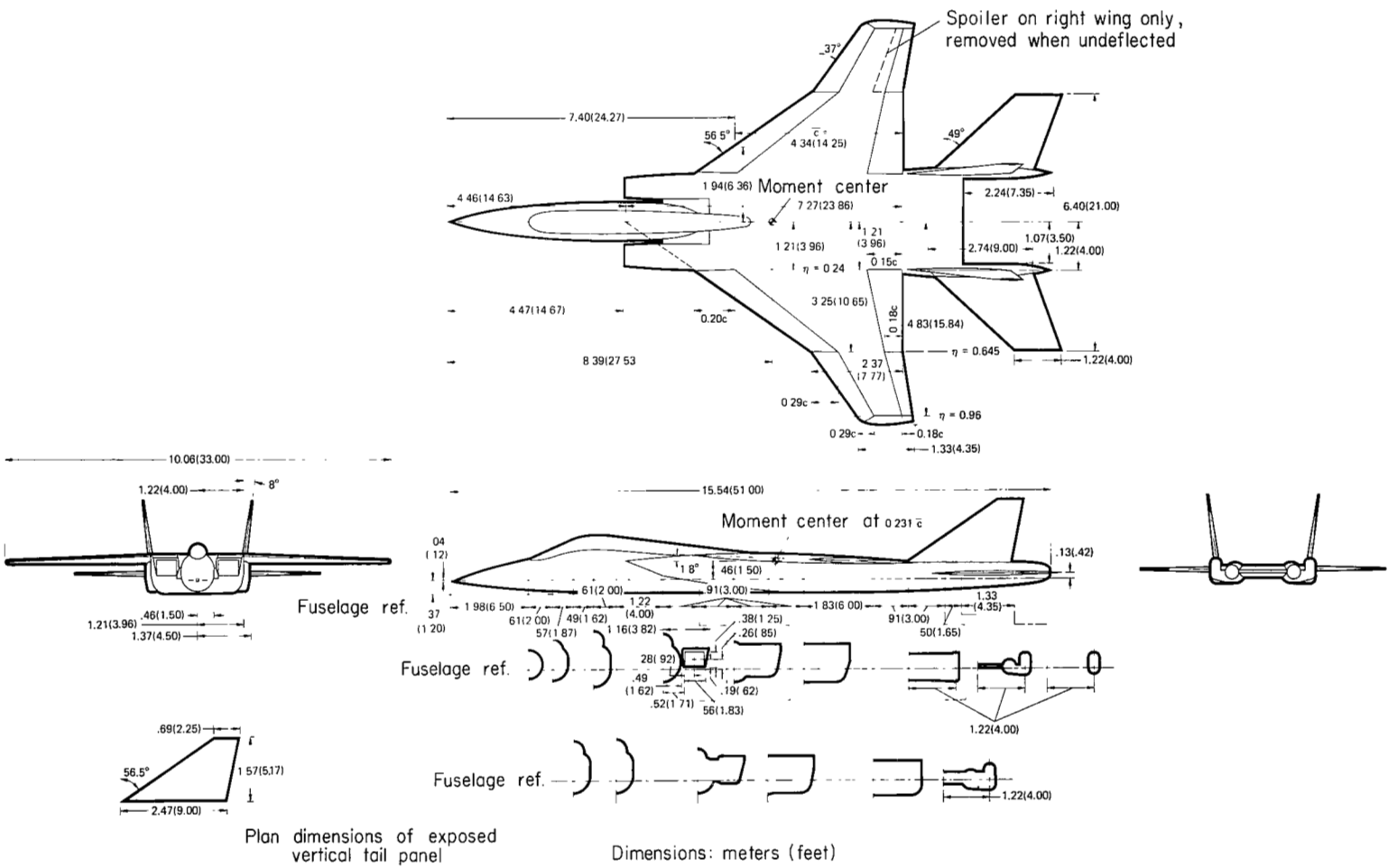

(a) Geometric details of model.

Figure 2.– Model dimensions and geometry.

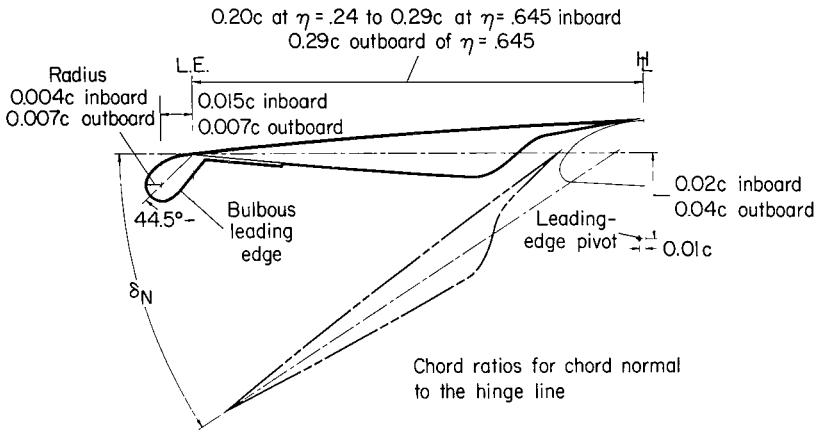

(b) Leading-edge flap details.

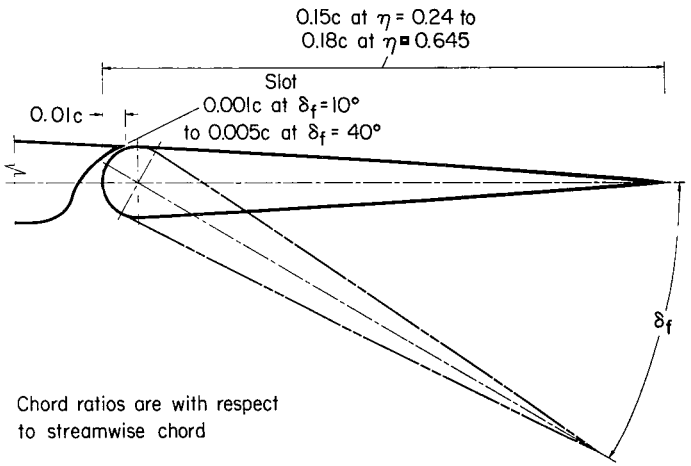

(c) Inboard trailing-edge flap details.

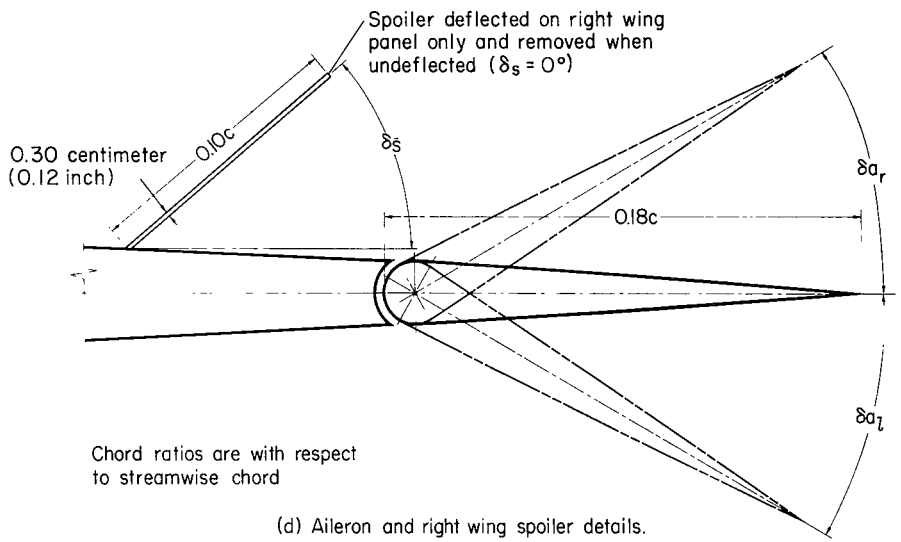

(d) Aileron and right wing spoiler details.

Figure 2.– Concluded.

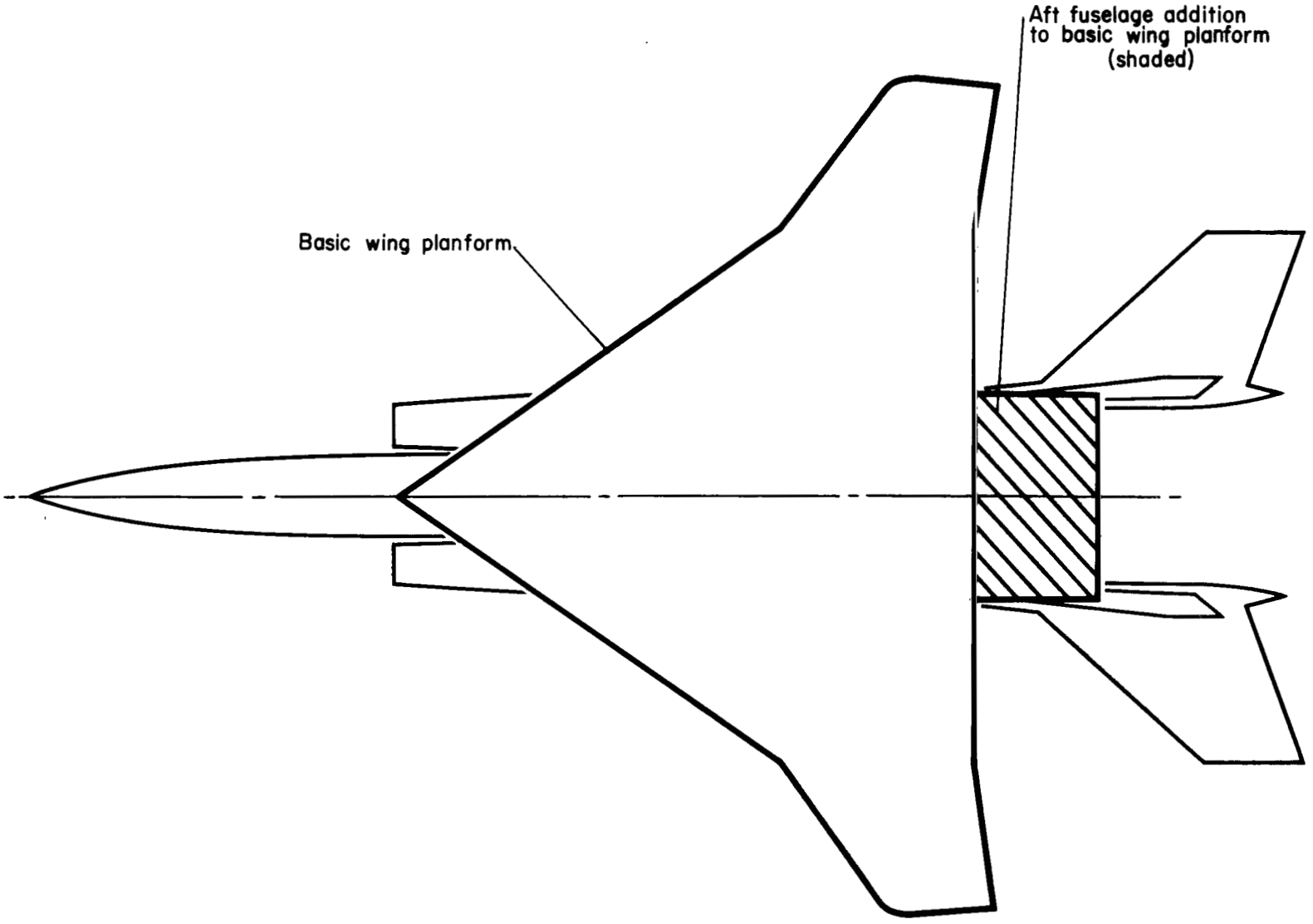

Figure 3.– Basic wing planform and the aft fuselage section comprising the total lifting planform used in the theoretical comparisons.

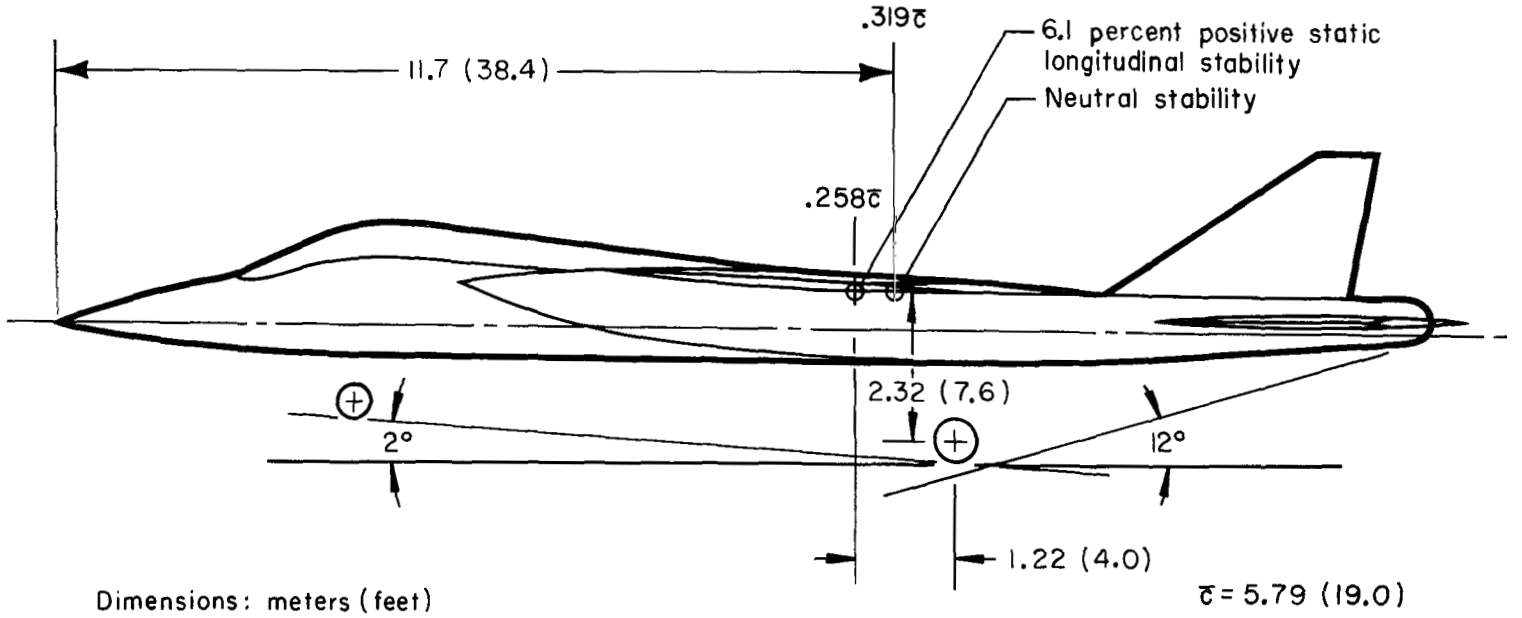

Figure 4.– Center-of-gravity locations and ground roll attitude of the 4/3 scale aircraft used to estimate takeoff performance.

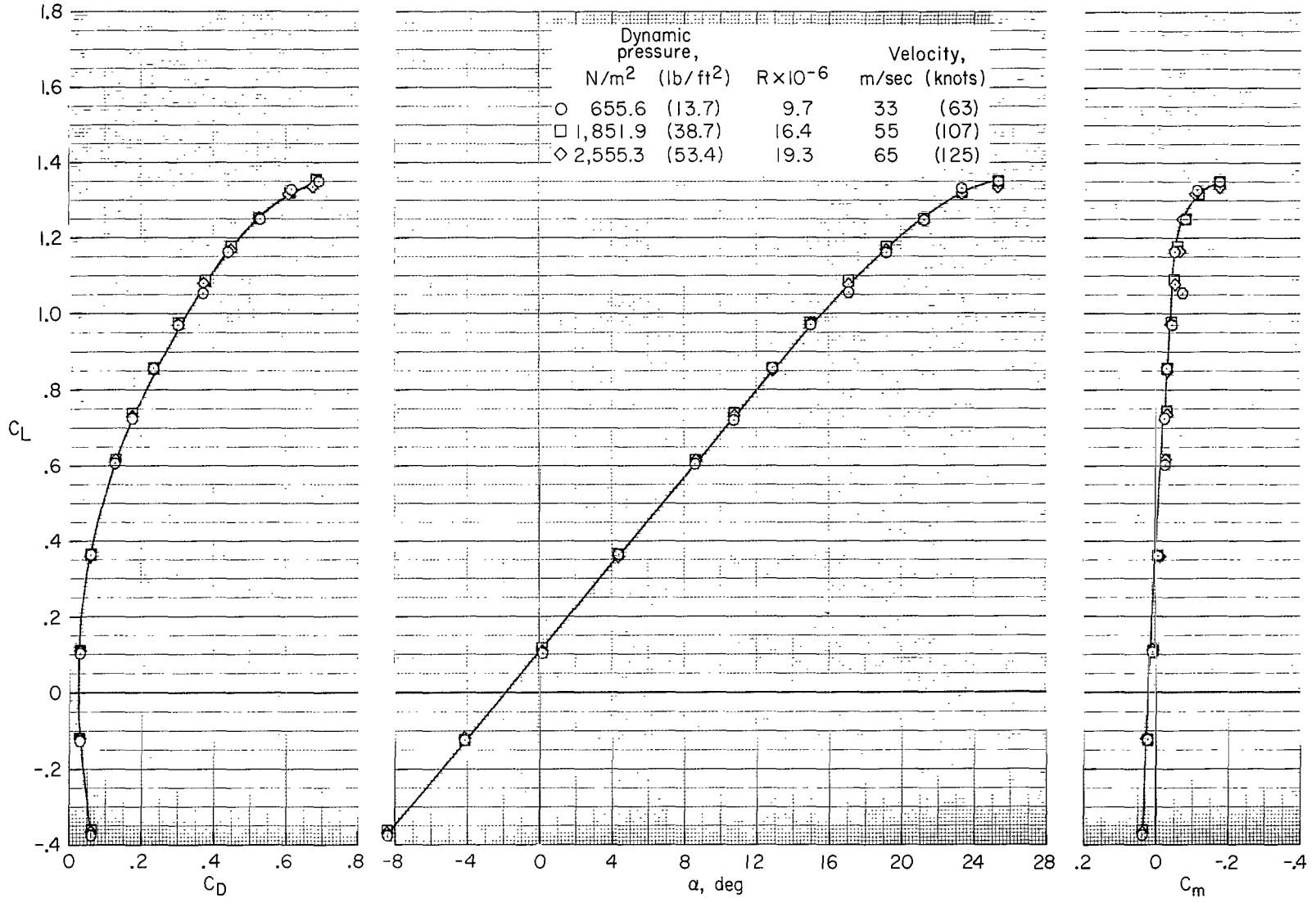

(a) Cruise configuration; $\delta_N = 0°$, $\delta_f = 0°$.

Figure 5.– Effect of Reynolds number variation on the longitudinal aerodynamic characteristics of the model; $\beta = 0°, i = 0°$.

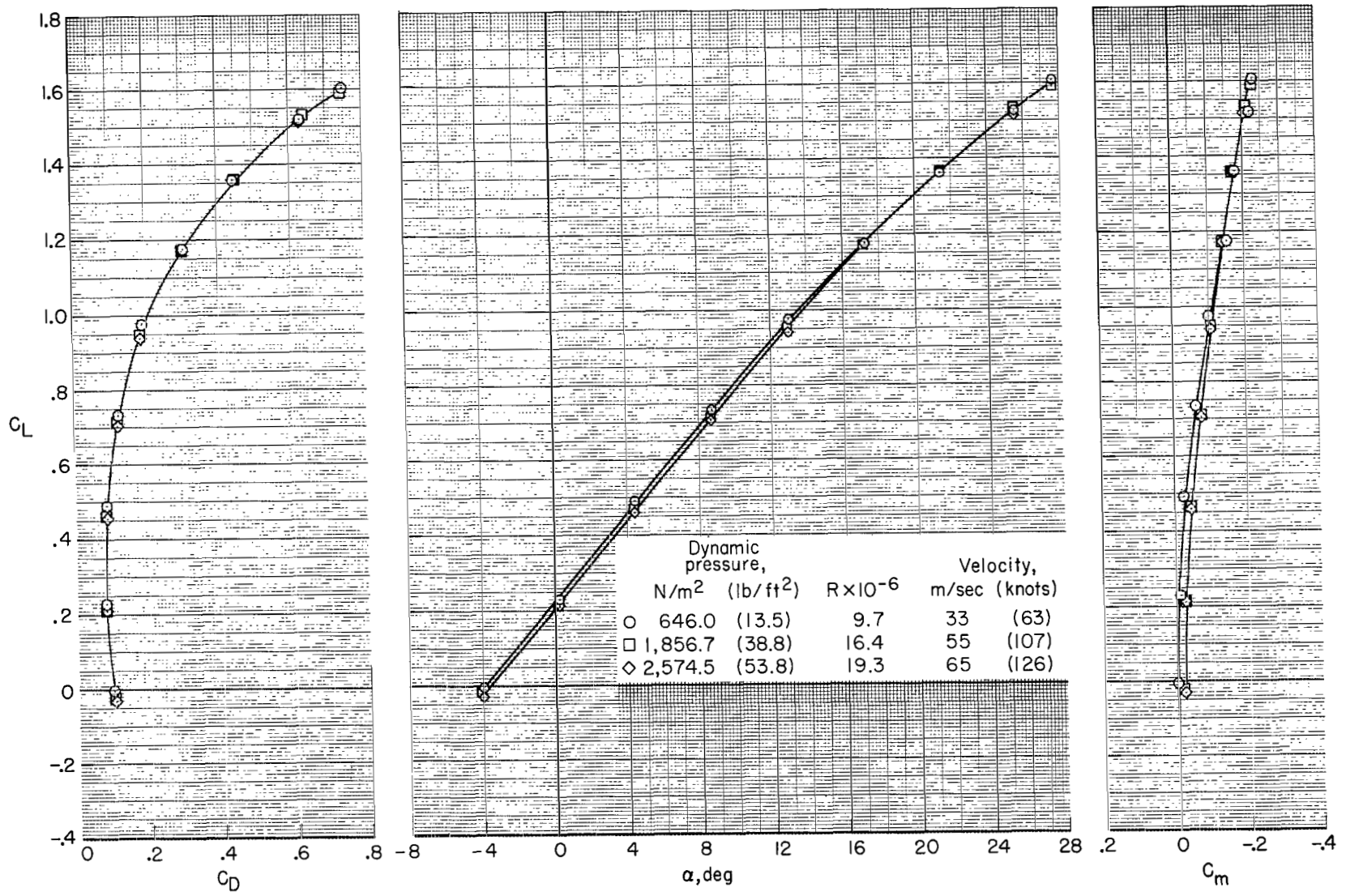

(b) High-lift configuration; $\delta_N = 50°/35°$, $\delta_f = 30°$.

Figure 5.– Concluded.

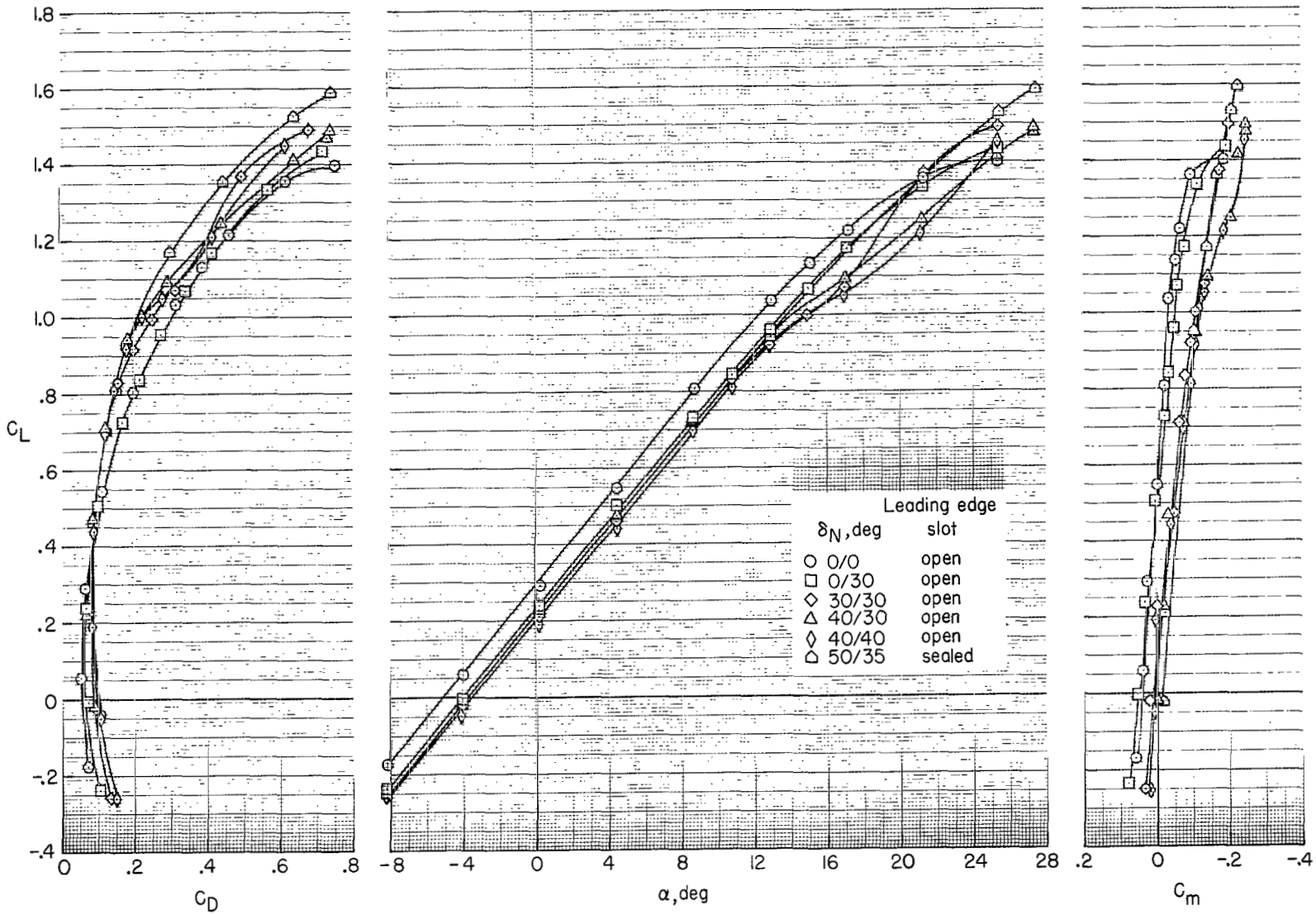

(a) Sharp leading edge.

Figure 6.– Effect of leading-edge flap deflection on the longitudinal aerodynamic characteristics of the model; $\delta_f = 30°$, $\beta = 0°$, $i = 0°$, $V = 55$ m/sec (107 knots).

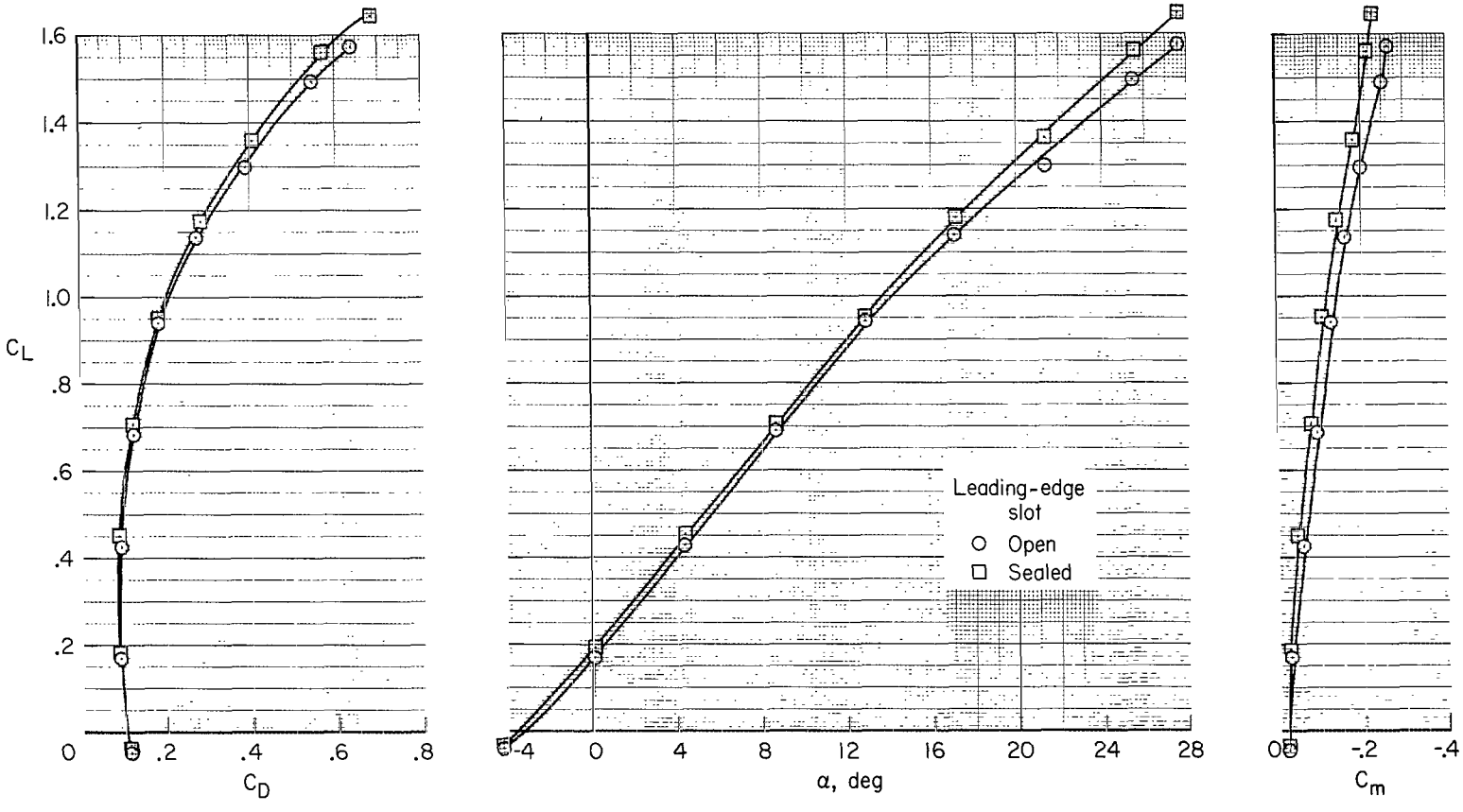

(b) Bulbous leading edge; $\delta_N = 50°/35°$.

Figure 6.– Concluded.

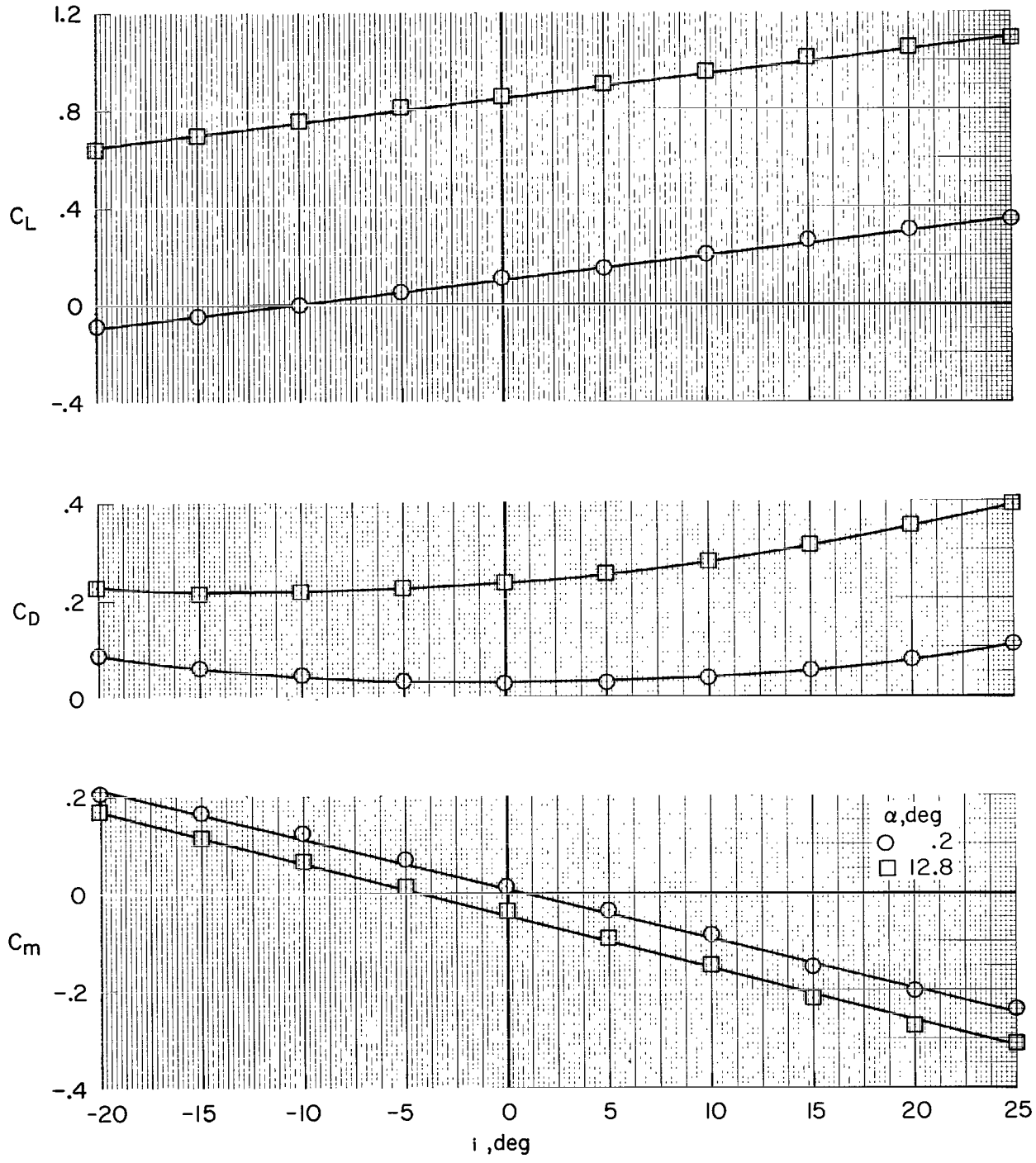

(a) Cruise configuration; $\delta_N = 0°$, $\delta_f = 0°$.

Figure 7.– Effects of horizontal-tail incidence on the model longitudinal aerodynamic characteristics; $\beta = 0°$, $V = 55$ m/sec (107 knots).

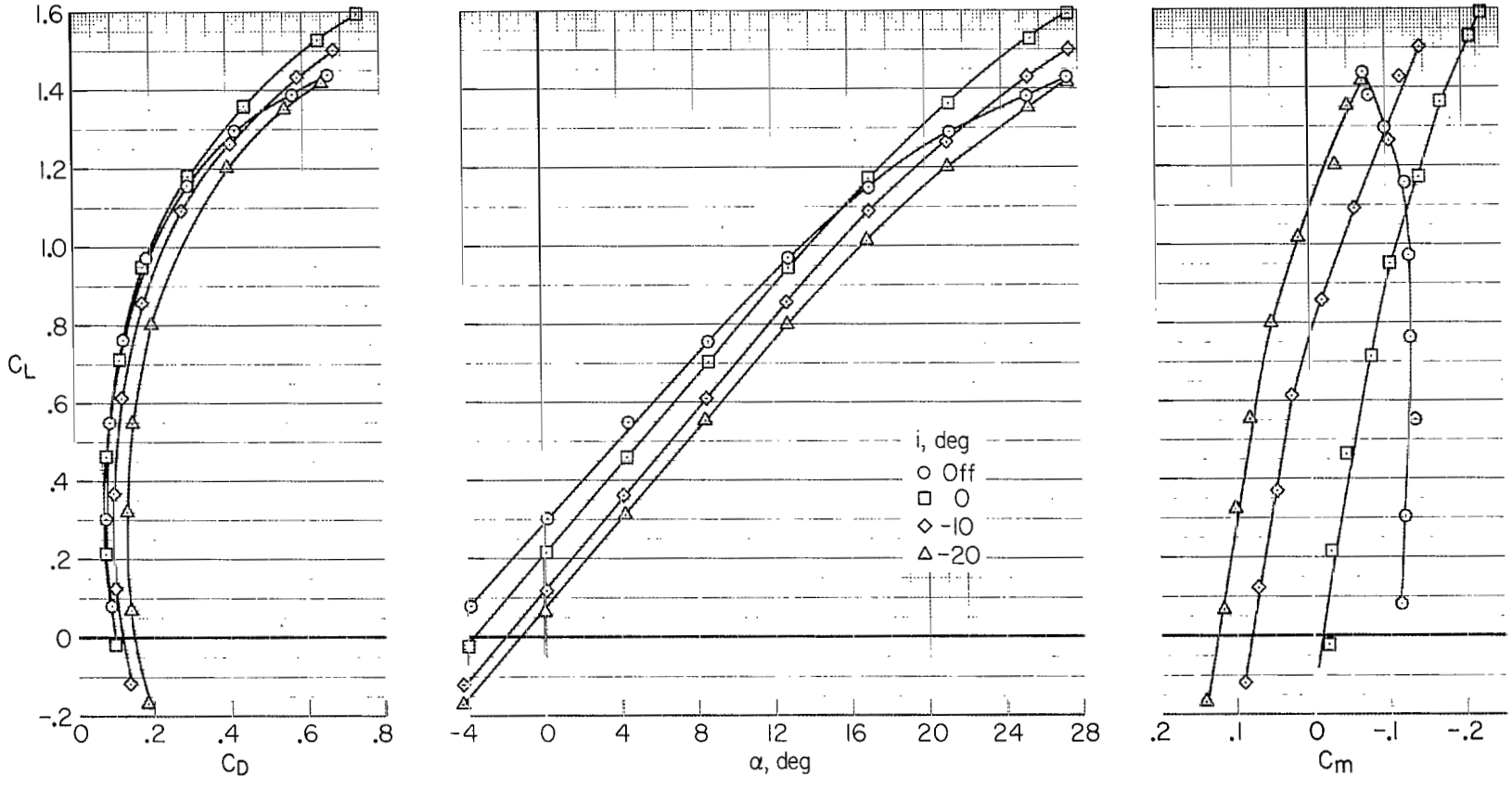

(b) High-lift configuration; $\delta_N = 50°/35°$, $\delta_f = 30°$.

Figure 7.– Concluded.

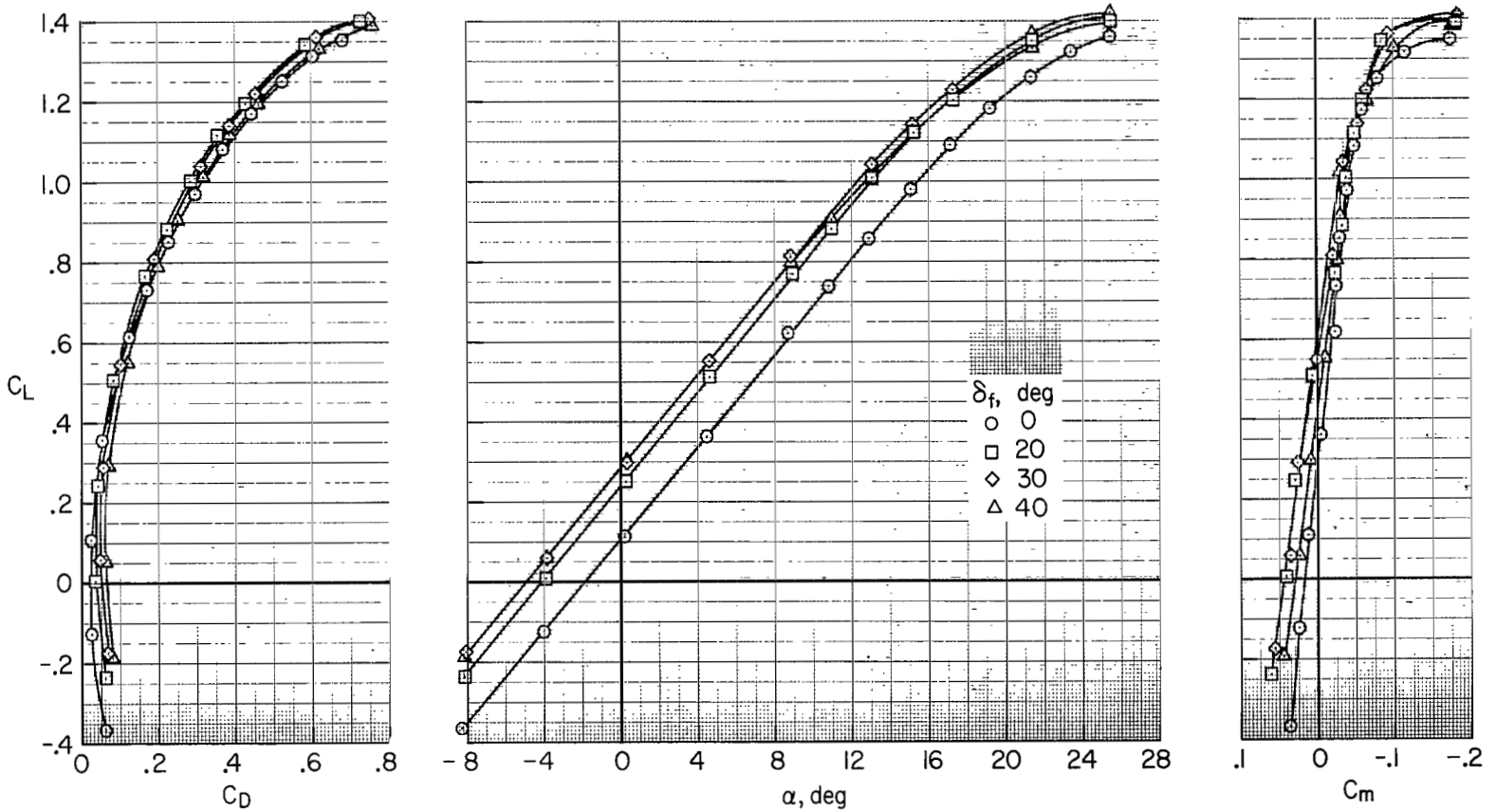

(a) Horizontal tails on; $i = 0°$.

Figure 8.– Effect of trailing-edge flap deflection on the longitudinal aerodynamic characteristics of the model; $\delta_N = 0°$, $\beta = 0°$, $V = 55$ m/sec (1 07 knots).

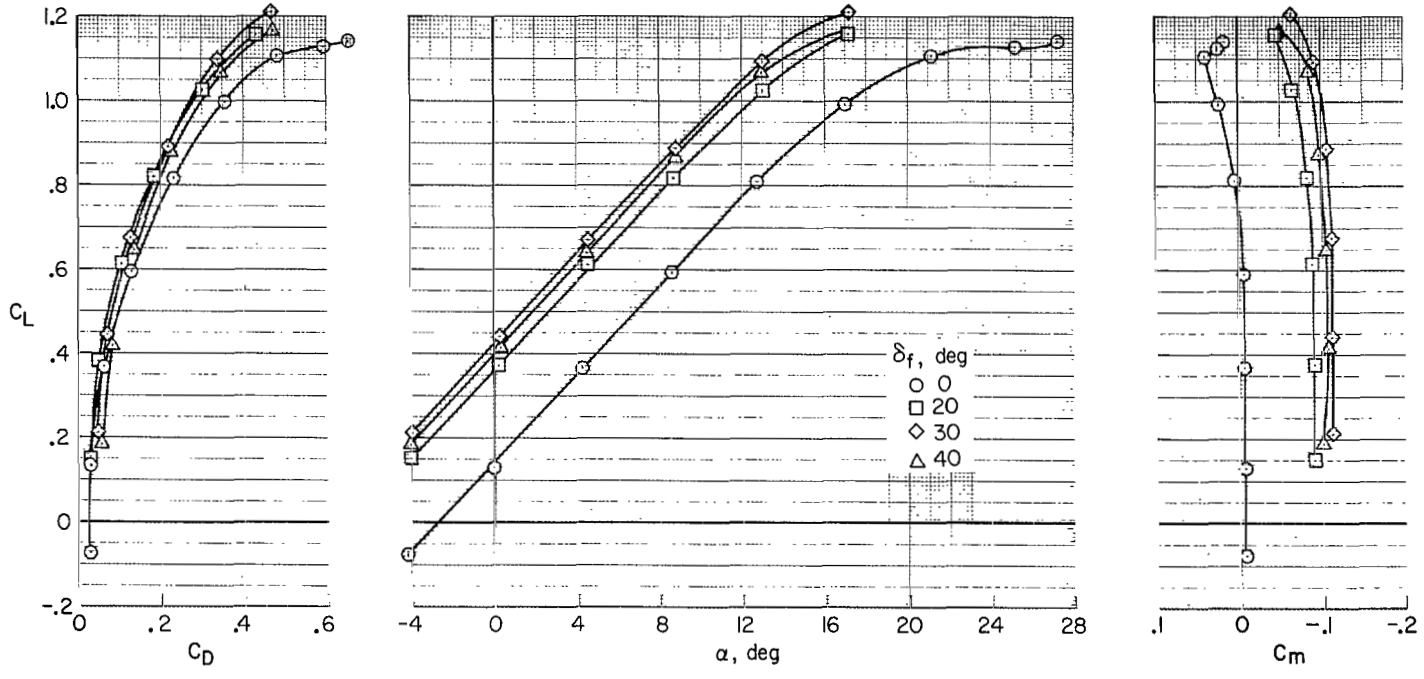

(b) Horizontal tails off.

Figure 8.– Concluded.

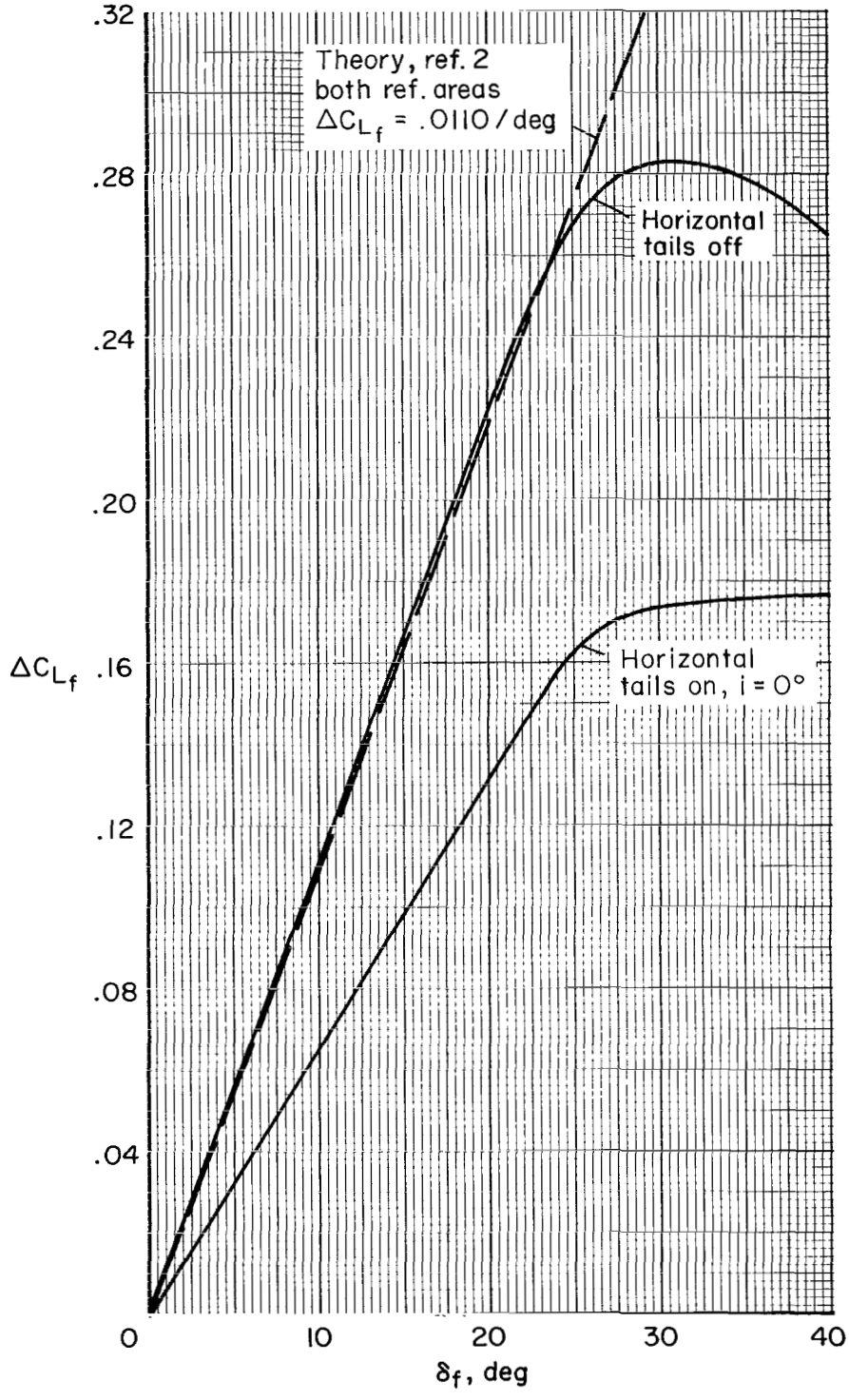

Figure 9.—Effect of horizontal tails on trailing-edge flap effectiveness; $\alpha = 0.28°$, $\delta_N = 0°$, $\beta = 0°$, $V = 55$ m/sec (107 knots).

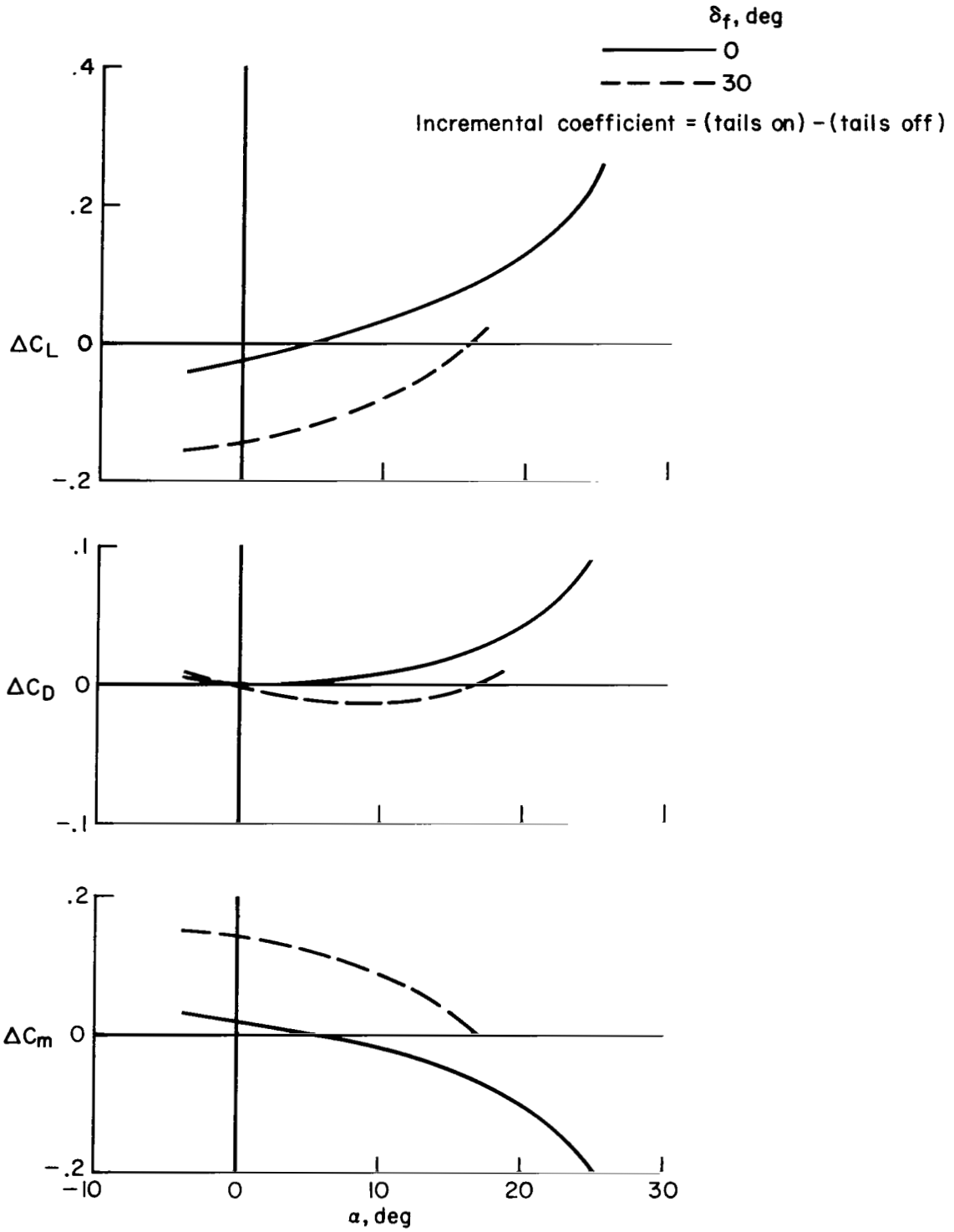

Figure 10.– Effect of 0° and 30° of trailing-edge flap deflection on the incremental contribution of the horizontal tails to the model longitudinal aerodynamic characteristics; $\delta_N = 0°$, $\beta = 0°$, $V = 55$ m/sec (107 knots).

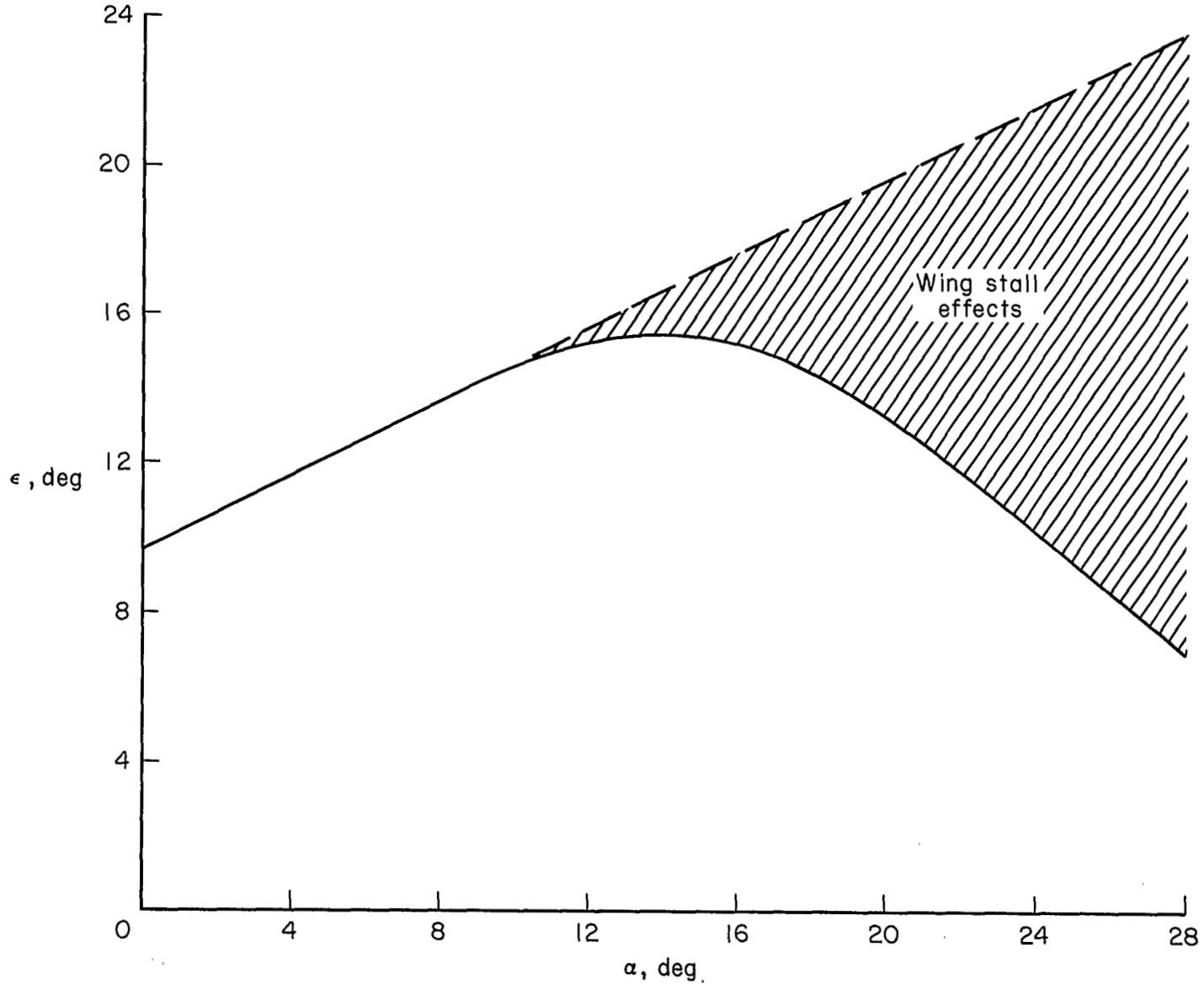

Figure 11.– Estimated downwash at the horizontal tails induced by 30° of trailing-edge flap deflection; $\delta_N = 50°/35°$, $\beta = 0°$, $V = 55$ m/sec (107 knots).

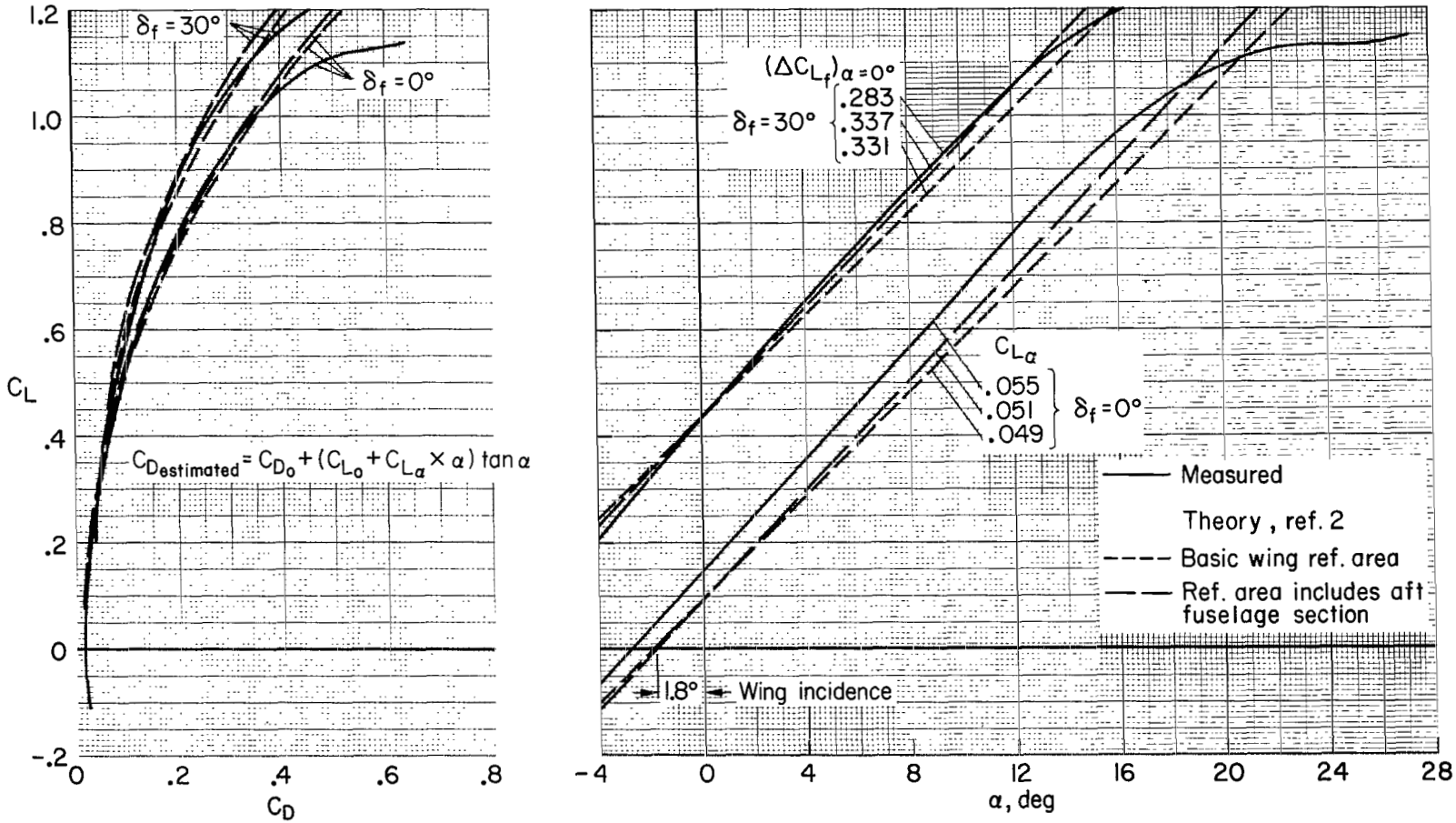

(a) Comparisons with theory of reference 2.

Figure 12.– Comparison of measured model lift and drag with that estimated from theory; horizontal tails removed, $\delta_N = 0°$, $\beta = 0°$, $V = 55$ m/sec (107 knots).

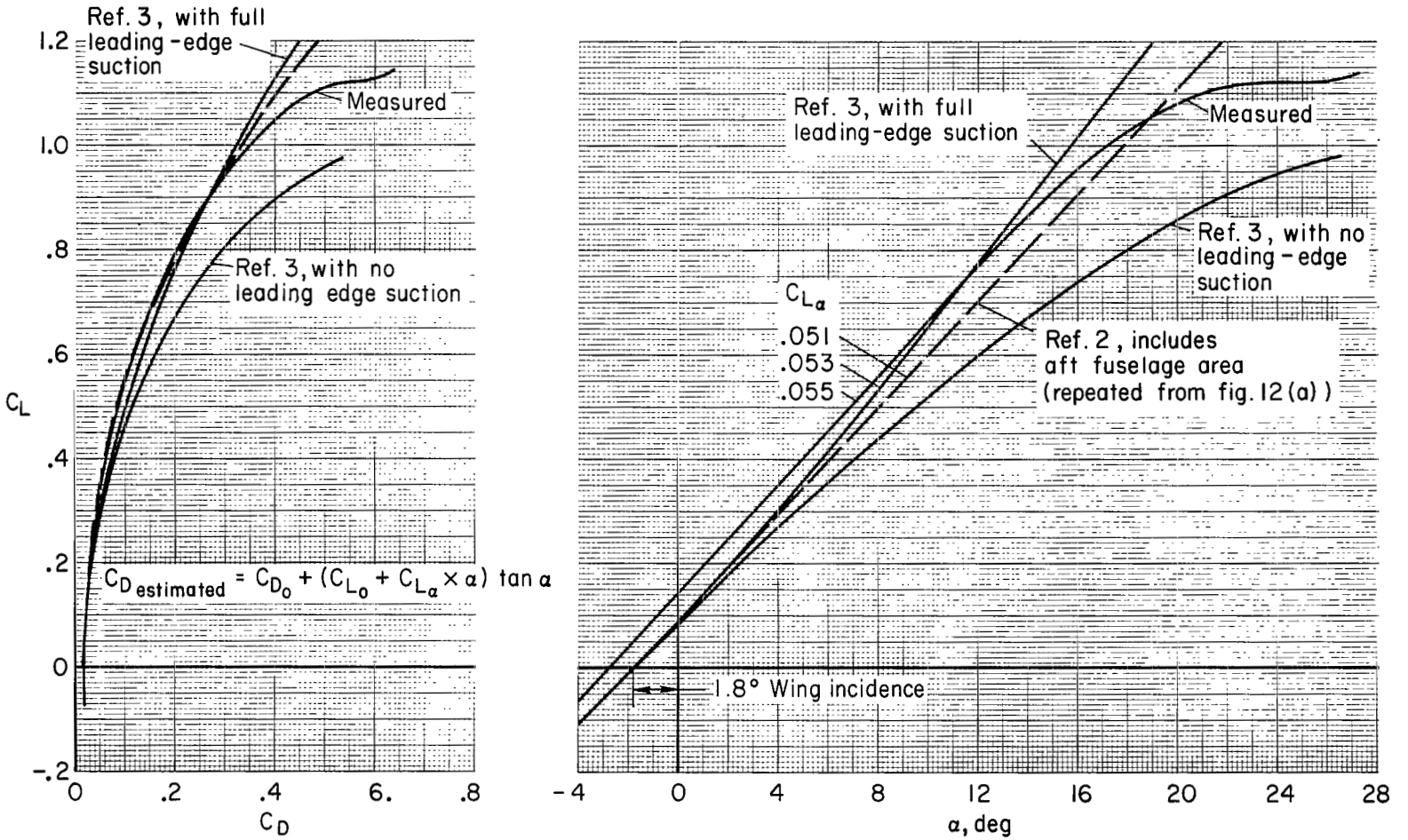

(b) Comparisons with theory of reference 3; $\delta_f = 0°$.

Figure 12.– Concluded.

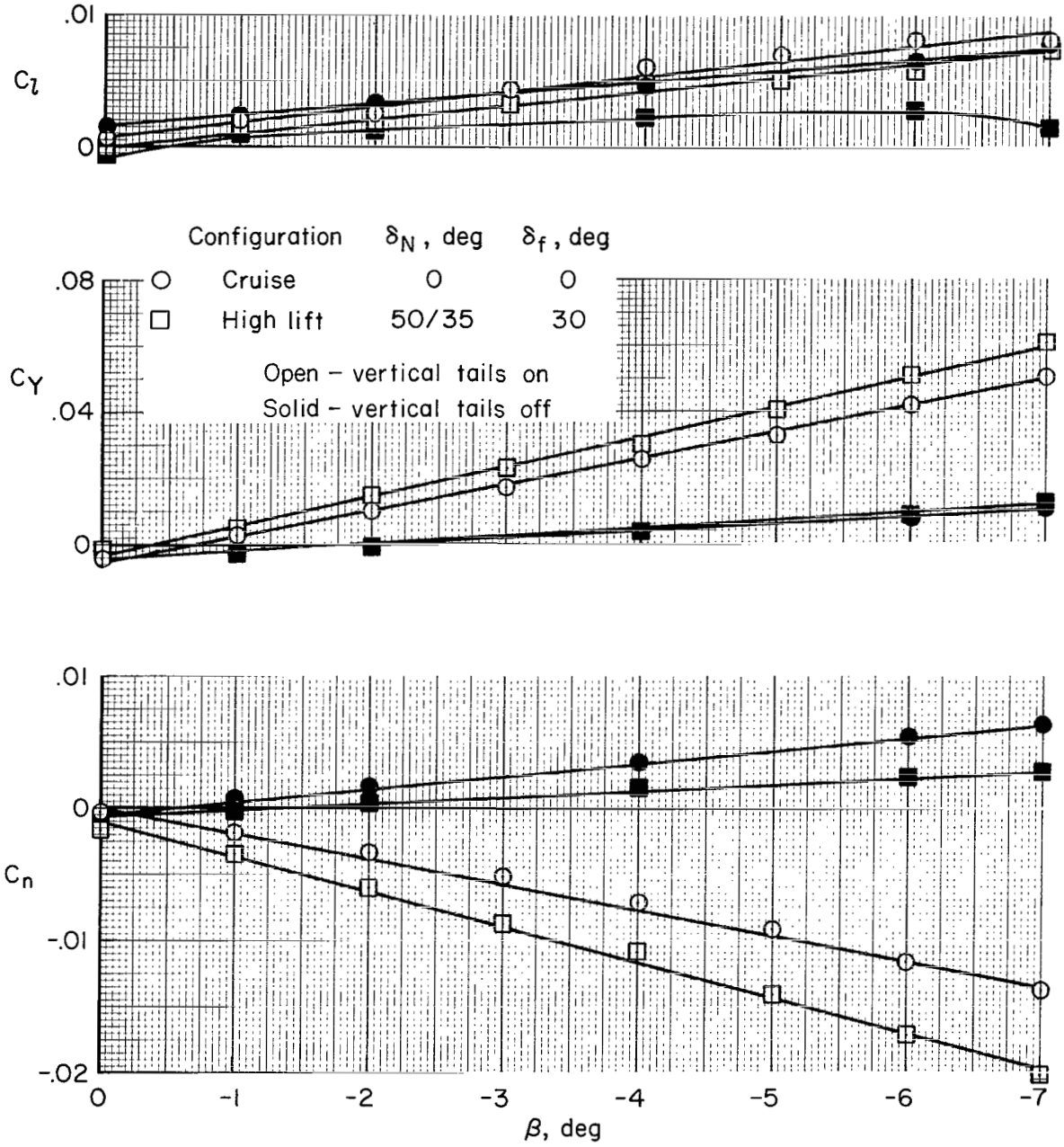

(a) $\alpha = 0.2°$.

Figure 13.– Contribution of vertical tails to the model lateral-directional aerodynamic characteristics with changes in sideslip; V = 55 m/sec (107 knots).

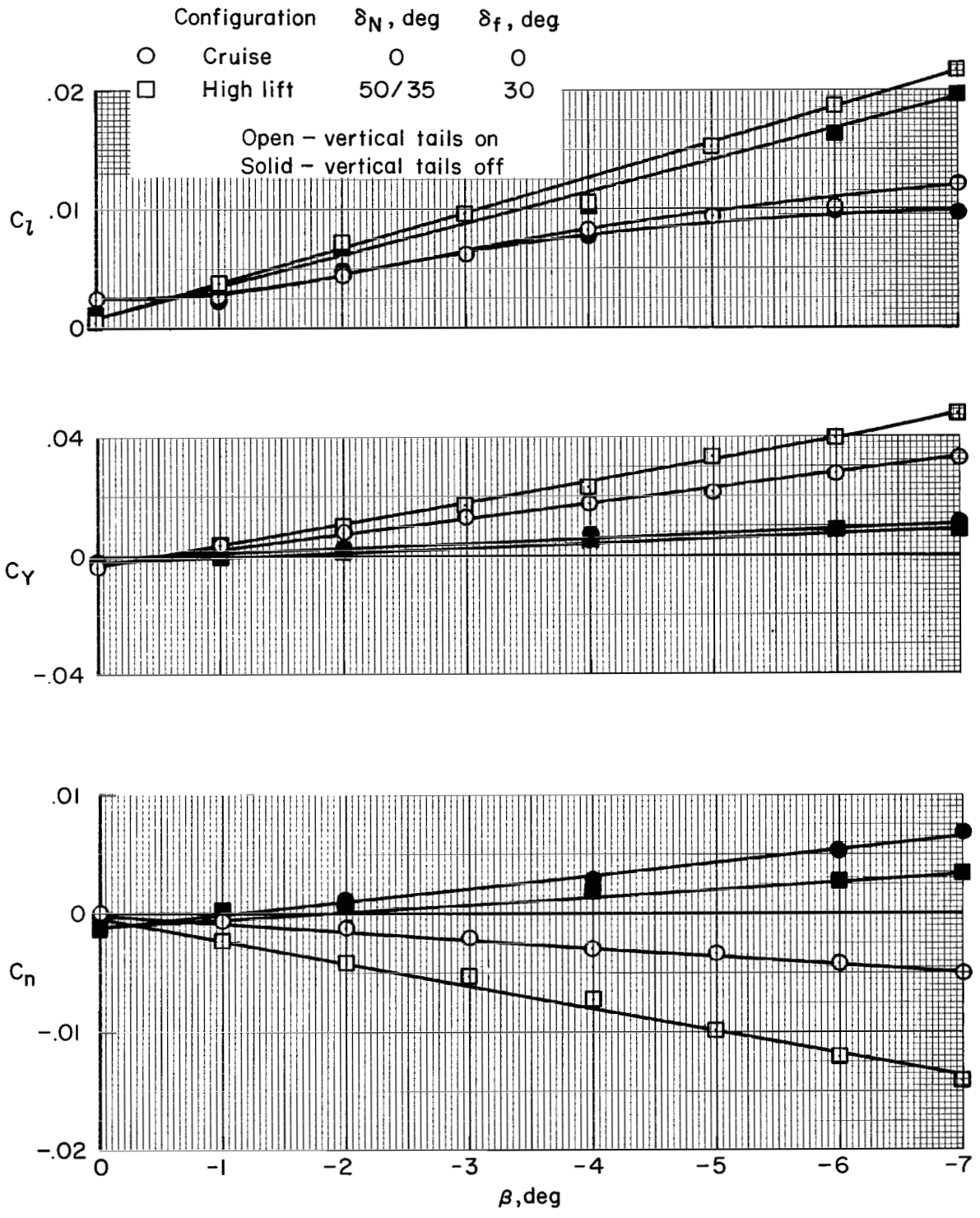

(b) $\alpha = 12.9°$.

Figure 13.– Concluded.

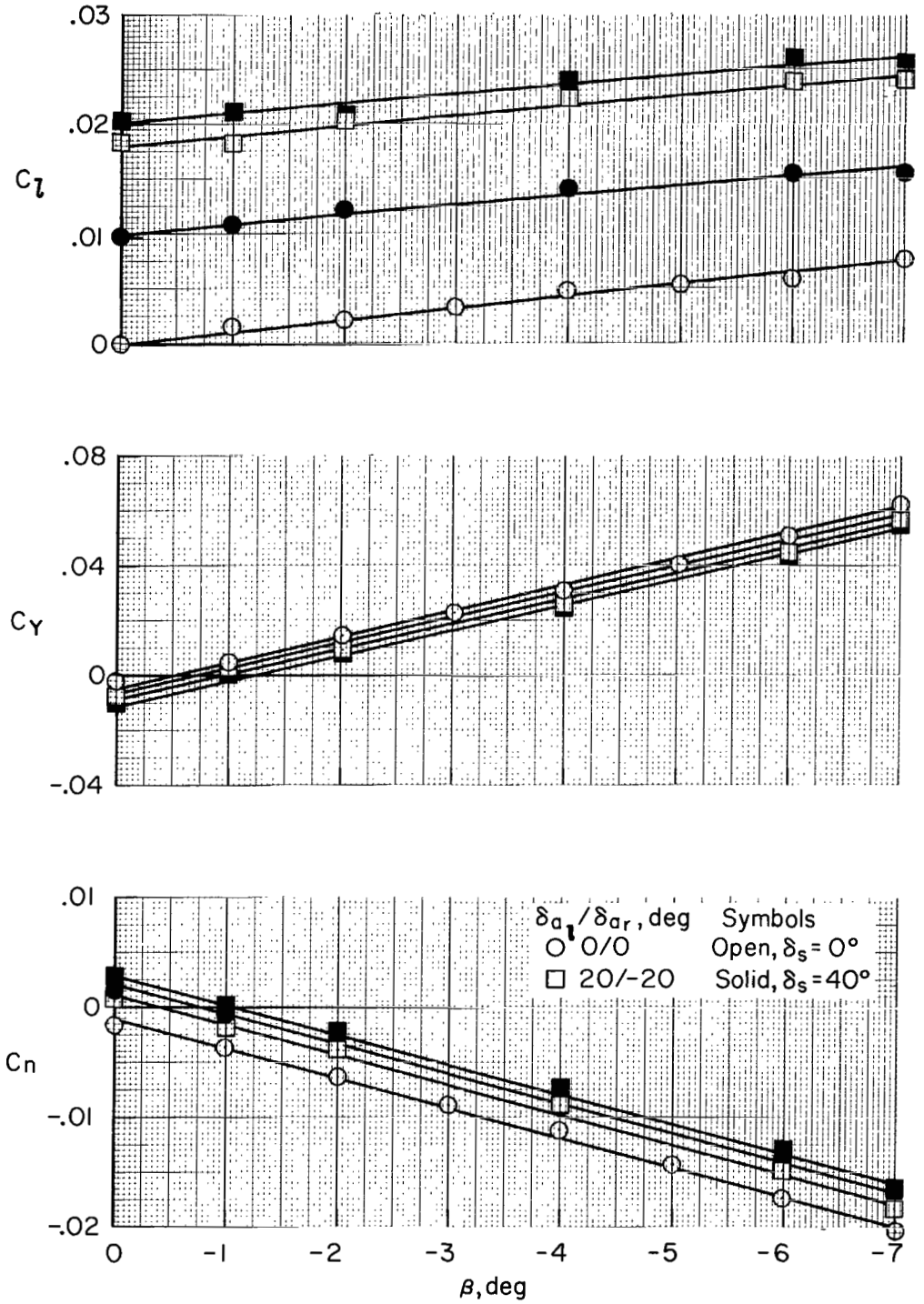

(a) $\alpha = 0.2°$.

Figure 14.– Effects of differential aileron and right wing spoiler deflection on the model lateral-directional aerodynamic characteristics at sideslip; $\delta_N = 50°/30°$, $\delta_f = 30°$, $V = 55$ m/sec (107 knots).

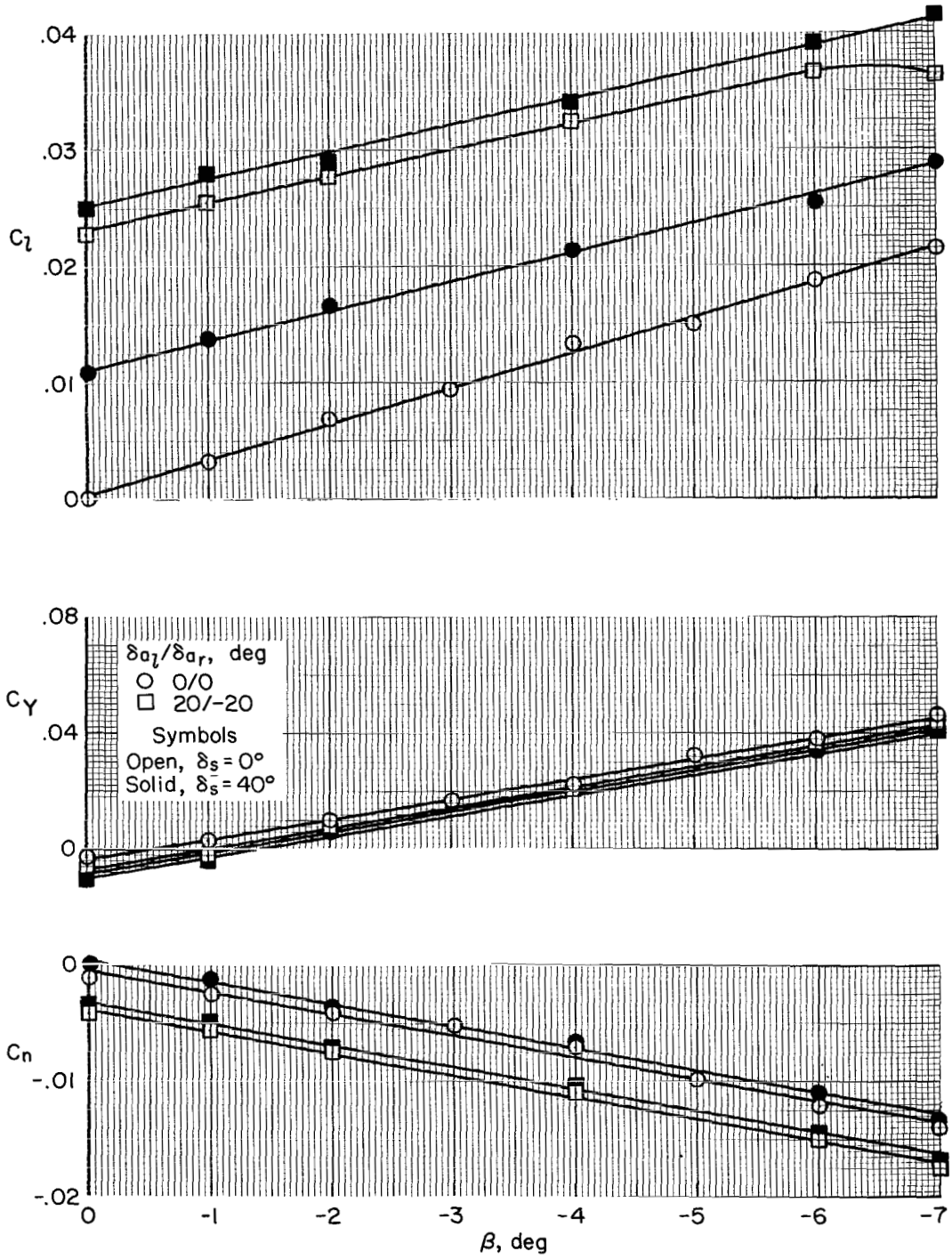

(b) $\alpha = 12.9°$.

Figure 14.– Concluded.

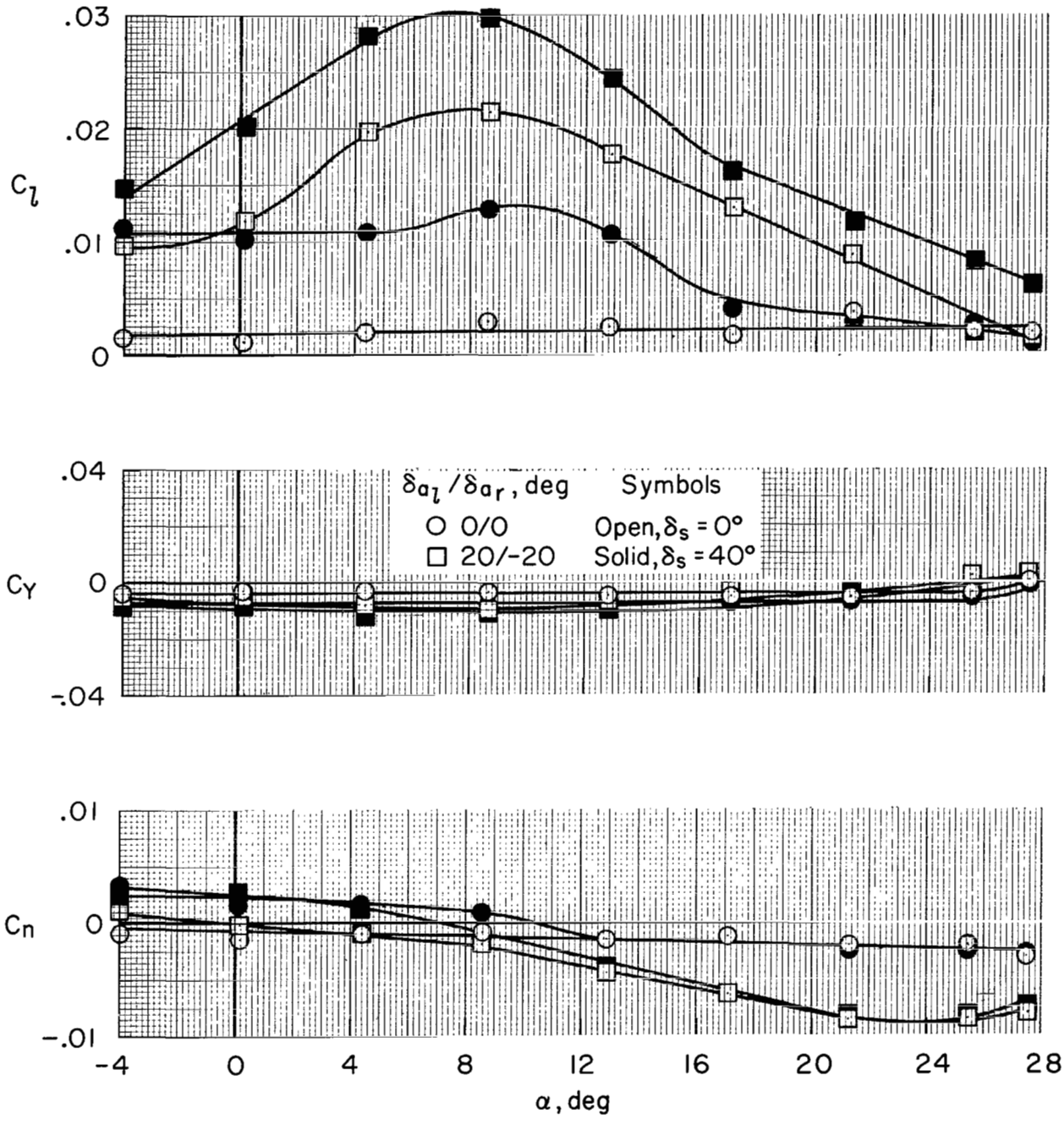

Figure 15.– Effects of differential aileron and right wing spoiler deflection on the model lateral-directional aerodynamic characteristics with changes in angle of attack; $\beta = 0°$, $\delta_N = 50°/35°$, $\delta_f = 30°$, $V = 55$ m/sec (107 knots).

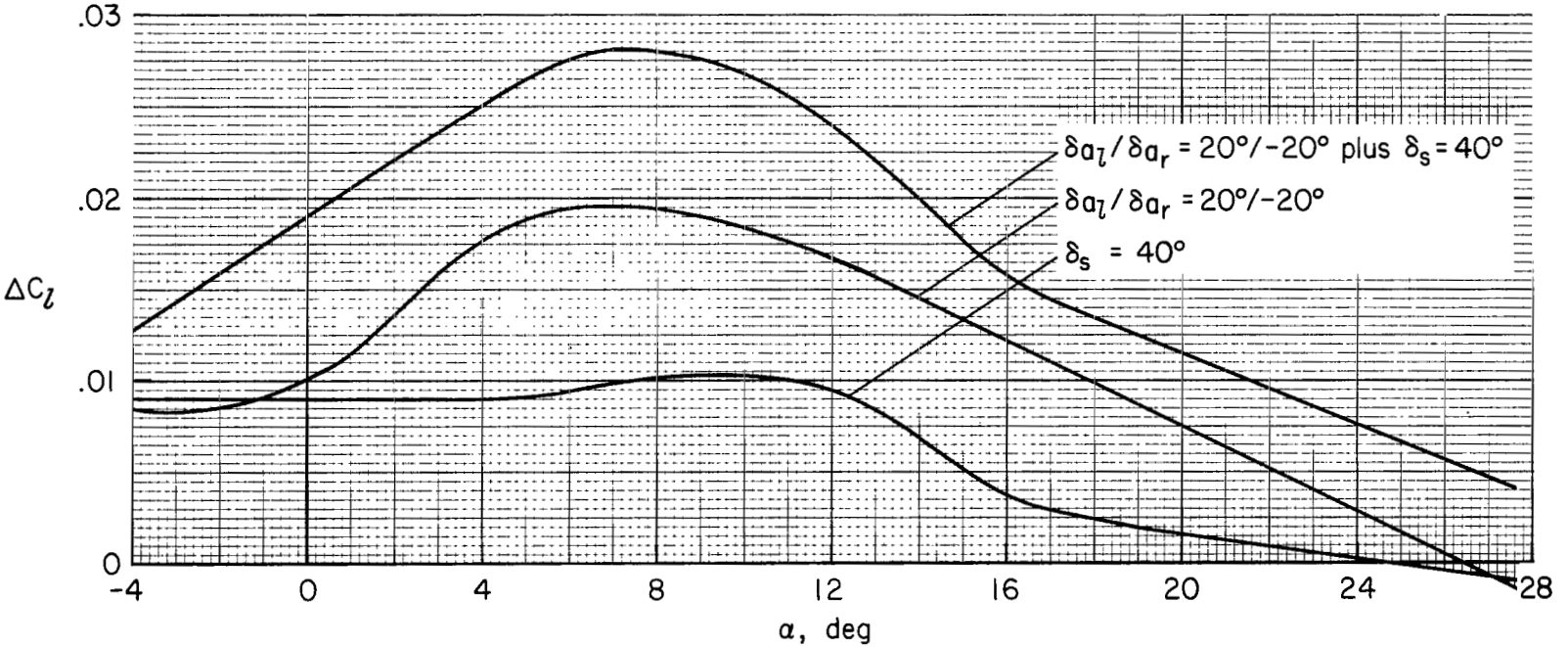

Figure 16.– Incremental variation of rolling-moment coefficient with changes in angle of attack for the model with the ailerons and right wing spoiler deployed as individual and combined controls; $\beta = 0°$, $\delta_N = 50°/35°$, $\delta_f = 30°$, $V = 55$ m/sec (107 knots).

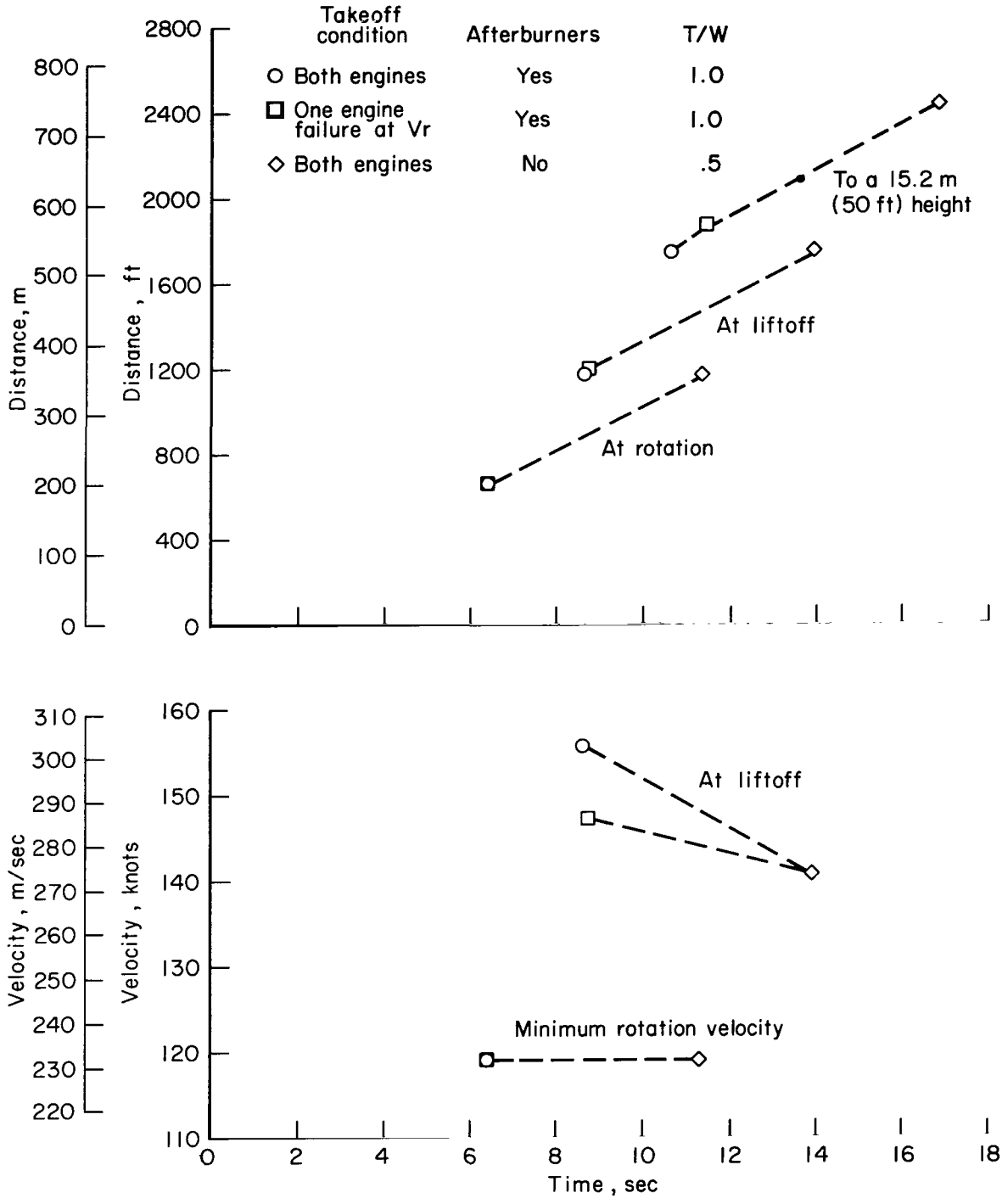

(a) Distance and velocity.

Figure 17.– Estimated takeoff performance of the full scale aircraft; W/S = 2873 N/sq m (60 psf), $dC_m/dC_L = -0.061$, $\delta_N = 50°/35°$, $\delta_f = 30°$.

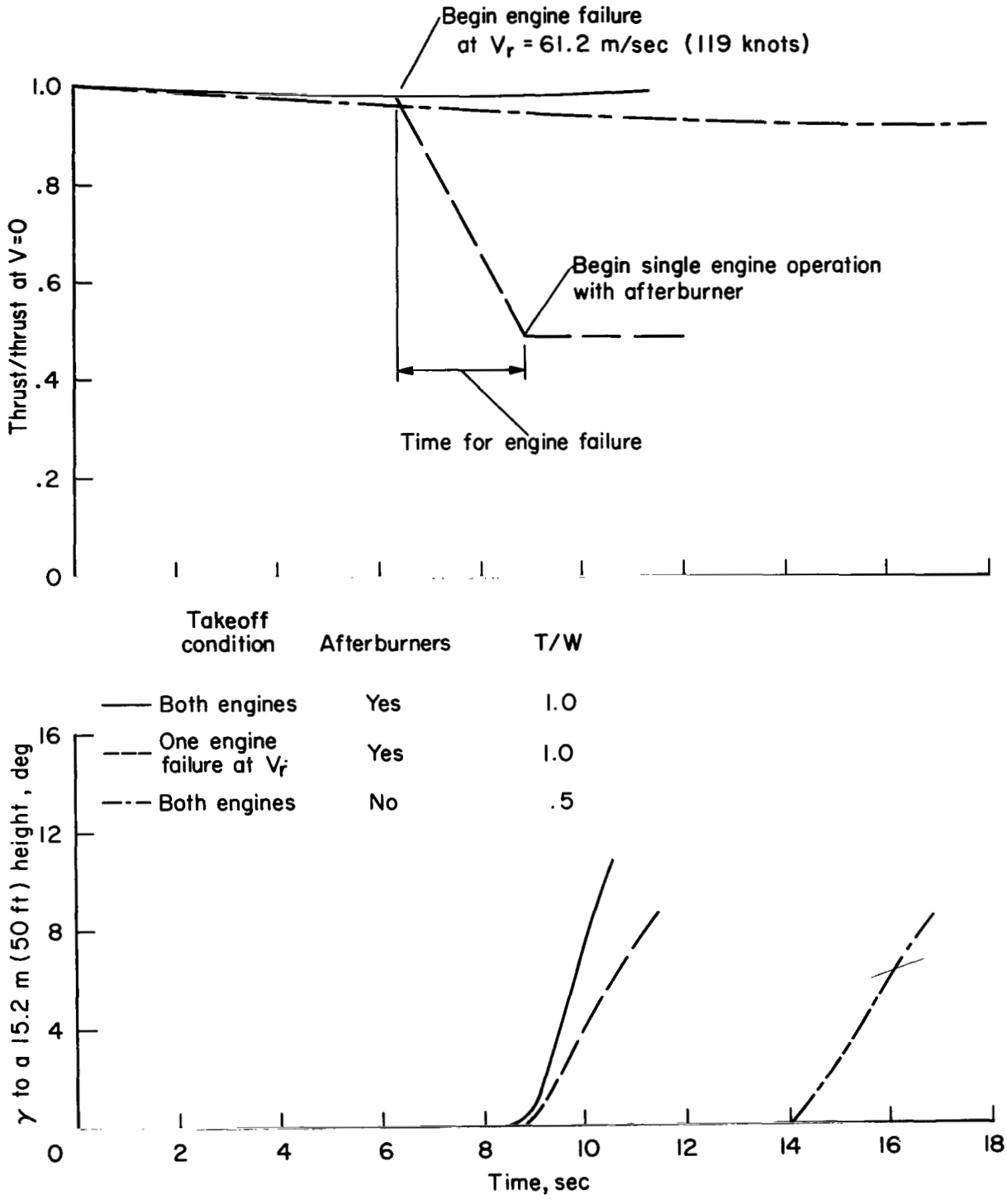

(b) Thrust and flight path angle.

Figure 17.– Concluded.

"The aeronautical and space activities of the United States shall be conducted so as to contribute . . . to the expansion of human knowledge of phenomena in the atmosphere and space. The Administration shall provide for the widest practicable and appropriate dissemination of information concerning its activities and the results thereof."

—NATIONAL AERONAUTICS AND SPACE ACT OF 1958

NASA SCIENTIFIC AND TECHNICAL PUBLICATIONS

TECHNICAL REPORTS: Scientific and technical information considered important, complete, and a lasting contribution to existing knowledge.

TECHNICAL NOTES: Information less broad in scope but nevertheless of importance as a contribution to existing knowledge.

TECHNICAL MEMORANDUMS: Information receiving limited distribution because of preliminary data, security classification, or other reasons.

CONTRACTOR REPORTS: Scientific and technical information generated under a NASA contract or grant and considered an important contribution to existing knowledge.

TECHNICAL TRANSLATIONS: Information published in a foreign language considered to merit NASA distribution in English.

SPECIAL PUBLICATIONS: Information derived from or of value to NASA activities. Publications include conference proceedings, monographs, data compilations, handbooks, sourcebooks, and special bibliographies.

TECHNOLOGY UTILIZATION PUBLICATIONS: Information on technology used by NASA that may be of particular interest in commercial and other non-aerospace applications. Publications include Tech Briefs, Technology Utilization Reports and Technology Surveys.

Details on the availability of these publications may be obtained from:

SCIENTIFIC AND TECHNICAL INFORMATION OFFICE

NATIONAL AERONAUTICS AND SPACE ADMINISTRATION

Washington, D.C. 20546